Title

Three-dimensional structure of the nicotinic acetylcholine receptor and location of the major associated 43-kD cytoskeletal protein, determined at 22 A by low dose electron microscopy and x-ray diffraction to 12.5 A.

Journal

Journal of Cell Biology, 109(2)

ISSN

0021-9525

Authors

Mitra, AK
McCarthy, MP
Stroud, RM

Publication Date

1989-08-01

DOI

10.1083/jcb.109.2.755

Three-Dimensional Structure of the Nicotinic Acetylcholine Receptor and Location of the Major Associated 43-kD Cytoskeletal Protein, Determined at 22 Å by Low Dose Electron Microscopy and X-Ray Diffraction to 12.5 Å

Alok K. Mitra, Michael P. McCarthy, and Robert M. Stroud

S-960 Department of Biochemistry and Biophysics, University of California in San Francisco, San Francisco, California 94143-0448

Abstract. The three-dimensional structure of the nicotinic acetylcholine receptor (AChR) from *Torpedo californica*, crystallized both before and after removal of associated proteins, most notably the main 43-kD cytoskeletal protein that interacts both with AChR and actin, is determined to a resolution of 22 Å. This is the first structural analysis where the 43-kD protein has been removed from the sample before crystallization. Thus, it provides the most reliable assessment of what constitutes the structure of the minimal five subunit AChR complex, and, by comparison with the native membrane, of the location of the 43-kD cytoskeletal protein.

Image reconstruction of two-dimensional crystals includes information from electron images of up to ±52° tilted specimens of latticed AChR. Hybrid density maps that include x-ray diffraction perpendicular to the membrane to 12.5 Å resolution were used and eliminate some of the distortions introduced in maps based only on electron microscopic analyses.

Comparison of the difference Fourier density maps between AChR with its normal complement of associated proteins, and without them shows that the main density, assigned to the actin-binding 43-kD component is closely associated with the lipid bilayer as well as with the cytoplasmic domain of the AChR. It binds beside the AChR, not beneath it as suggested by others (C. Toyoshima and N. Unwin 1988. *Nature [Lond.]*. 336:237–240). There is good agreement between the volumes of density for structural components and expected volumes based on their molecular weight.

Acetylcholine receptors aggregate in the absence of any cytoskeletal proteins, suggesting that the AChR alone is sufficient to encode and stabilize clustering, and perhaps to do so during synaptogenesis. The main 43-kD component may play a role in location and rate of association of AChR. We show that the disulfide bond that cross-links δ–δ chains of adjacent pentamers in about 80% of AChR, is not required to stabilize the lattice of AChR. Latticed tube structures are stable indefinitely. The lattices described here have 20% less volume of lipid than those originally obtained and characterized by J. Kistler and R. M. Stroud (1981. *Proc. Natl. Acad. Sci. USA.* 78:3678–3682), or those subsequently characterized by A. Brisson and P. N. T. Unwin (1984. *J. Cell Biol.* 99:1202–1211) and A. Brisson and P. N. T. Unwin (1985. *Nature (Lond.).* 315:474–477).

THE acetylcholine receptor is a 295-kD complex of five homologous transmembrane glycoprotein subunits (Raftery et al., 1980) arranged like staves around a central channel (Klymkowsky and Stroud, 1979; Kistler et al., 1982). The cylindrical 25-Å-diam entry well surrounded by protein extends ~55 Å above the membrane into the synapse and controls the electrostatic field upon approach of an ion to the narrowest part of the transmembrane pore (Klymkowsky and Stroud, 1979; Kistler et al., 1982; Toyoshima and Unwin, 1988) that lies in the center of the five-subunit complex (Kistler et al., 1982). The bilayer is 41 Å ± 1 Å thick between head groups (Ross et al., 1977; Stroud and Agard, 1979). The transmembrane part of the channel is ~40 Å long, and ~7 Å in diameter (Kistler et al., 1982) forming the narrowest parts of the ion-conducting channel.

Gating of the acetylcholine receptor (AChR)[1] may be provided in part by tight ion-binding sites that are located within the transmembrane portion of the resting channel (Fairclough et al., 1986). Neurotoxins, which lock the channel closed (Jackson, 1984) and compete with acetylcholine for high

Dr. McCarthy's present address is the Department of Pharmocology, University of Medicine and Dentistry of New Jersey and the Center for Advanced Biotechnology and Medicine, Piscataway, NJ 08854.

1. *Abbreviations used in this paper*: AChR, acetylcholine receptor; BgTx, bungarotoxin; CTF, contrast transfer function.

affinity sites on the α-subunits of the receptor are located on the top crest of the synaptic rim (Klymkowsky and Stroud, 1979; Fairclough et al., 1983).

Upon binding agonists, the ion channel is opened, allowing the influx of ~10^4 sodium ions/ms/AChR into the cell, and the consequent depolarization of the post-synaptic membrane (Anderson and Stevens, 1973; Neher and Sakman, 1976). The conformational changes associated with binding of the agonist carbamylcholine seem to be small as assessed by tritium-hydrogen exchange. This is the case for desensitizing concentrations of carbamylcholine (>10 μM). Only slightly larger changes accompany treatment with activating concentrations (<10 μM) (McCarthy and Stroud, 1989*a*). The small changes upon desensitization have been characterized in three dimensions by Unwin et al. (1988). More significant changes occur in the part of the protein that is in contact with the lipid bilayer and surrounds the ion conducting channel as assessed by a dramatic decrease in labeling from the lipids by the lipophilic diazirine 3-trifluoromethyl-3-iodophenyl diazirine (White and Cohen, 1988; McCarthy and Stroud, 1989*b*). Neurotoxins α-bungarotoxin and curare induce much larger changes in conformation and so must close down channel function by a mechanism other than either stabilizing the resting state or desensitization (McCarthy and Stroud, 1989*a*).

The subunit arrangement around the channel is unique. The alpha chains are separated by one other subunit (Holtzman et al., 1982; Zingsheim et al., 1982; Fairclough et al., 1983; Bon et al., 1984; Kubalek et al., 1987). Based on immuno-electron microscopy, the most accurately measured angular distance between equivalent epitopes on the two α-subunits is 144° ± 4° (n * 360°/5) (Fairclough et al., 1983), consistent with a quasi-symmetrical and nearly precise pentameric arrangement (Fairclough et al., 1983). The subunit arrangement, $\alpha\beta\alpha\gamma\delta$ clockwise as seen from the synapse, was deduced from immunoelectron microscopy using specific anti-α-subunit Fab fragments of monoclonal antibodies, and chemical cross-linking (Kistler et al., 1982; Fairclough et al., 1983). The possibility of chemical cross-linking not necessarily being to nearest neighbors renders it indirect. Further evidence in favor of the same arrangement of subunits, placed in the crystal unit cell have been inferred on the basis of projection difference maps generated between AChR in the presence of Fab fragments of monoclonal anti-AChR antibodies, wheat germ agglutinin, and α-bungarotoxin (Kubalek et al., 1987). Problems with the recognized cross-reactivity of anti-subunit antibodies and penetration of the antibody fragments into the generally sealed vesicles render these procedures also indirect. Nevertheless, the subunit arrangement is an agreed consensus at this time.

AChR and the Cytoskeleton

In the mature synapse, the AChR is found to be associated with a number of different components, but stoichiometrically so with only one principal component, a 43-kD protein that has actin binding capacity. The other minor AChR-associated cytoskeletal proteins have roles in linking AChR to the cytoskeleton, in clustering of AChR, and in provision of ATP near regions where the Na^+/K^+ ATPase is also concentrated (Froehner, 1986). There is no solid evidence that any of these proteins regulate the activity of AChR. We show here that AChR alone, after removal of the cytoskeletal components still encodes the ability to aggregate in ordered fashion in vitro in the membrane. It is possible that this may play a role in synaptogenesis. We show direct evidence for a close association between the 43-kD protein and cytoplasmic domains of AChR.

Clusters of AChR, which form simply with time in the absence of synaptic interactions in tissue culture (Prives et al., 1982; Stya and Axelrod, 1983), accumulate at sites of innervation along the postsynaptic membrane (Ziskind-Conhaim et al., 1984). Within these regions, the AChR is apparently bound and immobilized, through interactions both with the basal lamina (Bayne et al., 1984; Olek et al., 1986) and with the cytoskeleton (Cartaud et al., 1981, 1982). The linkage between the AChR and the cytoskeleton and other associated proteins can be released by treatment at pH 11.0 for 1 h. These extrinsic membrane proteins can then be separated from the sample in a subsequent step (Neubig et al., 1979). Specifically, a class of proteins having a relative molecular mass 43,000 D are removed, typically referred to as the 43-kD, or ν_1, ν_2, and ν_3 proteins, which can be distinguished by isoelectric focussing. ν_2 and ν_3 are minor components and have been shown to be cytosolic (Gysin et al., 1981), with ν_2 identified as creatine kinase and ν_3 as actin (Gysin et al., 1983). ν_1 (herein to be referred to as 43-kD protein) has been identified as the major component of the "subsynaptic density" (Caraud et al., 1981) observed at sites of innervation on muscle and *Torpedo* electric organ by specific labeling with monoclonal antibodies raised against the ν_1 43-kD protein (Froehner et al., 1981; Nghiem et al., 1983) and exists at the synapse at ~1:1 stoichiometry with the AChR (LaRochelle and Froehner, 1986). There is evidence, on nitrocellulose, that the 43-kD protein binds actin (Walker et al., 1984). A close interaction with the AChR is also suggested by chemical cross-linking studies, where the 43-kD protein has been found to cross-link specifically to the β subunit of the AChR (Burden et al., 1983). cDNAs encoding two 43-kD proteins, differing in their carboxy termini, have been isolated and cloned from *Torpedo californica* electroplax (Frail et al., 1987). These genes and proteins show no homology with any other available sequences.

Removal of the 43-kD protein, by alkaline extraction, increases the rotational (Lo et al., 1980; Rousselet et al., 1982) and translational (Barrantes et al., 1980) mobility of the AChR, and lessens its heat stability (Saitoh et al., 1979). (It is not possible in any of these studies to separate the effects of incubating the AChR for 1 h at pH 11.0, typical conditions for alkaline extraction, from those effects resulting from removal of the 43-kD protein). These observations are in accord with the general picture that synaptic AChR is immobilized through interactions with both the basal lamina and the cytoskeleton, and that the 43-kD protein acts as a noncovalent cross-linker between the AChR and the cytoskeleton, perhaps by binding to actin.

Three-Dimensional Structure of AChR

Electron microscopy and x-ray diffraction have already provided an understanding of the three-dimensional shape of the AChR, (Kistler et al., 1982; Stroud and Finer-Moore, 1985; Toyoshima and Unwin, 1988) and evidence for bundles of oriented α-helices within the complex (Ross et al., 1977; Stroud and Finer-Moore, 1985). Rosettes of 70–80-Å diameter seen in the postsynaptic membrane (Nickel and Potter,

1973; Cartaud et al., 1973; Cartaud et al., 1978) were shown to be AChR using immuno-electron microscopy (Klymkowsky and Stroud, 1979), where it was also demonstrated that the neurotoxin binding sites lie on the top crest of the AChR. Ross et al. (1977) described and characterized uranyl acetate-stained AChR in projection, in ordered, two-dimensional crystalline sheets. Kistler and Stroud (1981) first discovered and characterized two-dimensional AChR crystals found in tubular vesicles from *T. californica* with 43-kD protein present. In combination with x-ray diffraction data a hybrid three-dimensional structure was derived (Kistler et al., 1982). Our tube lattices were not then well enough ordered to justify a full electron micrographic 3-dimensional analysis. Better ordered tubes were obtained from *T. marmorata* (Brisson and Unwin, 1984). These permitted Brisson and Unwin (1984, 1985) to include diffraction from tilted specimens and analyze frozen, hydrated samples wherein the cross section of the membrane-spanning regions of the protein are evident. Determination of the boundaries of the membrane-spanning regions, however, required the comparison of both stained and unstained specimens since the bilayer in these *T. marmarota* tubes was not visible. Omission of the sucrose density gradient used by Kistler and Stroud (1981) yielded the better-ordered material from *T. californica* we discuss here. In all previous structural analyses, approximately equimolar amounts of the 43-kD protein, and lesser amounts of other proteins, were present (though not always acknowledged to be present) and account for some of the density observed on the cytoplasmic surface as we now show.

After this manuscript was submitted, Toyoshima and Unwin (1988) reported helical reconstruction of ice-embedded tubes and of already formed tubes dialyzed against pH 11 immediately before freezing. In that case, while the associated proteins probably are loosened, they are not physically removed from the sample. In view of the sealed nature of many of the tube-containing vesicles, and the strong affinity of 43-kD protein for other proteins, it is likely that the associated proteins are still present inside the tubes. In our case the 43-kD proteins were removed from the system before tube formation. Thus, ours is the only analysis of tubular crystals where the associated proteins have been removed before crystallization.

Here we describe the biochemistry of both native and alkali-stripped samples containing tubular crystals and compare the AChR structure with that where the interactions with the associated proteins are maintained during the crystallization. Recent reviews of AChR structure and function include McCarthy et al., 1986; Stroud and Finer-Moore, 1985; Popot and Changeux, 1984; and Conti-Tronconi and Raftery, 1982.

Materials and Methods

Sample Purification

Samples of AChR-rich membrane fragments were prepared using modifications of the techniques of Klymkowsky et al. (1980) and Kistler and Stroud (1981), but without the sucrose density gradient sedimentation since we find that this produces better-ordered lattices. 60 g of excised electric organ from *T. californica*, either fresh or after storage in liquid nitrogen, was homogenized in 120 ml of chilled homogenization buffer (400 mM NaCl, 5 mM EDTA, 5 mM EGTA, 5 mM iodoacetamide, 0.2 mM PMSF in EtOH, 0.02% NaN_3, 10 mM Na H_2PO_4, pH 7.4, filtered through a 0.2-μm pore size filter [Nucleopore Corp., Pleasanton, CA]) in a homogenizer (model No. 23; Vir Tis Co., Inc., Gardiner, NY) for 4 min. The crude homogenate was centrifuged for 15 min at 6,500 rpm in an SS-34 rotor (DuPont Co., Wilmington, DE), and the resulting supernatant was collected through 8 layers of cheesecloth. The filtered supernatant was centrifuged for 55 min at 19,500 rpm in an SS-34 rotor and the pelleted membrane fractions suspended in K buffer (1 mM EDTA, 1 mM EGTA, 0.2 mM PMSF, 0.02% NaN_3, 10 mM Na H_2PO_4, pH 7.8, filtered through a 0.2-μm pore size filter (Nucleopore Corp.).

For quantitative removal of the 43-kD and associated proteins from the sample before crystallization, a portion of the native, suspended membrane fraction was again taken through the low speed/high speed centrifugation cycle described above, and the resulting membrane pellet was resuspended in distilled water. The pH was adjusted to 11.0 by the addition of dilute NaOH, to allow for the extraction of extrinsic membrane proteins as described by Neubig et al. (1979), and incubated for 1 h at 22°C. The membranes were pelleted by high speed centrifugation and resuspended in K buffer. SDS-PAGE confirmed that the 43-kD protein had been completely removed from the samples to be set up for crystallization.

Aliquots from both native and stripped membrane preparations were diluted to ~1–2-mg/ml protein, brought to 50 mM in $CaCl_2$, and incubated at 2°C for growing ordered vesicular tubes. Suspensions were assayed periodically for the appearance of ordered vesicles. Aliquots of the vesicle solutions were taken at these times and frozen at −20°C, for subsequent biochemical analysis.

Functional Assays

Protein concentration was determined using the procedure of Lowry et al. (1951) as modified for membrane proteins by Markwell et al. (1978). 0.1% SDS/10% polyacrylamide gels were run on a gel apparatus (Mini-Protean II; Bio-Rad Laboratories, Cambridge, MA) following the protocol of Laemmli (1970). α-bungarotoxin (BgTx) was either prepared by us from lyophilized snake venom, essentially following the protocol of Mebs et al. (1972), or purchased from Sigma Chemical Co., (St. Louis, MO). [^{125}I]-BgTx was purchased from Amersham Corp. (Arlington Heights, IL), and its binding to the AChR was measured by the filter binding assay of Schmidt and Raftery (1973) using DE81 discs from Whatman Inc. (Clifton, NJ).

Electron Microscopy

400-mesh copper grids covered with parlodian, and overlayed with a thin carbon film, were rendered hydrophilic by glow-discharge in air. A 5-μl sample applied to a grid was allowed to settle for 30 s, and then blotted dry with filter paper. Subsequently, the grid was washed 4 times on drops of distilled water, blotted dry between each wash, stained with 0.2% uranyl-acetate (pH 4.5) for 5 s, and blotted. Electron microscopy was carried out using an accelerating voltage of 80 kV on a microscope with a low dose kit (EM 400; Phillips Electronic Instruments, Eindhoven, Holland).

Grids were scanned for suitable looking vesicles at 2,500× magnification, and ordered vesicles were imaged at 40,540× magnification under low-dose conditions. The actual magnification was standardized in each case from unit cell dimensions of uranyl acetate stained images of beef liver catalase (Unwin, 1975). The electron dose for recording images was set to be under 20 $e^-/Å^2$ using a dose-calibrated electrometer connected to the viewing screen. To minimize radiation damage, no more than five images were recorded from a single tube. Images were recorded on film (4489; Eastman Kodak Co., Rochester, NY) developed for 4 min in 4 times normal developer (D19; Eastman Kodak Co.) strength to increase effective film sensitivity under low dose conditions. To obtain three-dimensional data specimens were tilted by prescribed angles up to ±52° and imaged at 9,000–17,000 Å underfocus. The degree of underfocus was calculated from the positions of the Thon rings (Thon, 1971), using the manufacturer-provided spherical aberration coefficient of 3.6 mm. The degree of order of AChR in vesicles was assessed by optical diffraction and selected regions were digitized on a flatbed scanning densitometer (1010M; Perkin Elmer Corp., Norwalk, CT) using a 20 μm aperture and step size equivalent to 5 Å in the object.

Three-Dimensional Image Reconstruction

Digitized regions of AChR arrays were displayed on an image processor (6400; Gould/DeAnza Co., San Jose, CA), and well-preserved areas, typically 200 × 300 pixels, were floated and padded to 512 × 512 pixels, and then Fourier transformed. Since the helical, crystalline vesicles flatten on the grid, both sides are superposed in the image. An example of separation and indexation of the diffraction patterns from the two faces of the flattened

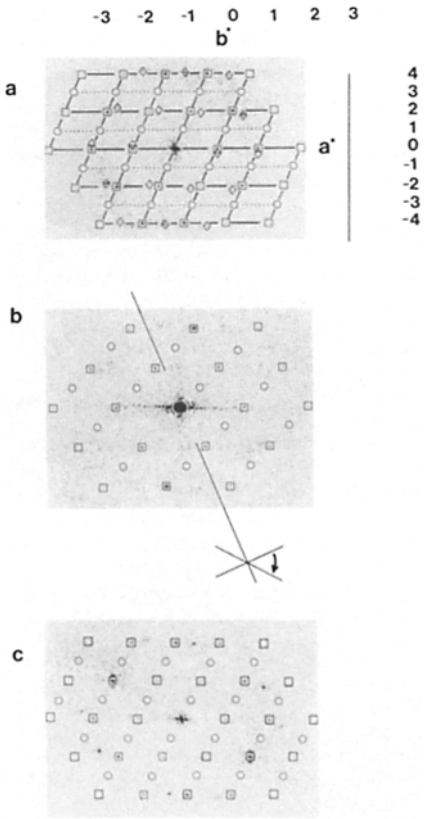

Figure 1. Computed Fourier transforms from ordered tubular arrays of AChR. (*a*) The central region of the transform from an untilted native acetylcholine receptor array is indexed. The vertical line indicates the direction of the long axis of the tube. (*b*) The diffraction pattern from the same array after it had been tilted by 52° around the indicated axis. (*c*) The central region of diffraction from an untilted acetylcholine receptor array crystallised after 43-kD and associated proteins had been removed. In each case, indexing of the better preserved lattice is indicated. Projection amplitudes and phases are listed in Table I. Open squares surround the strong peaks and open circles surround the weak (*hk*) reflections with k = odd. These contain information that corresponds to the difference between the two molecules in the unit cell. Also indicated in *a*, with open diamonds, are the reflections arising from the less well-preserved lattice. The length of the vertical line (*a*) corresponds to 0.05614 $Å^{-1}$.

vesicle is shown in Fig. 1 *a*. The lattice whose extra-cellular face is in contact with the grid always showed better preservation of order, particularly at high angles of tilt (Fig. 1 *b*), and this one was chosen for all subsequent image reconstruction. The reciprocal lattice parameters were refined by least-squares minimization of the difference between observed and calculated reflection positions. For projection data, the amplitude, phase, and figures of merit were determined by intensity-weighted averaging over the peaks of each reflection (Ross et al., 1977). The well-preserved area of each image was corrected for crystal-lattice distortions, an idea first described and applied in reciprocal space by Hayward and Stroud (1981), but now following the real space protocol of Henderson et al. (1986) as modified by Robinson et al. (1988). Based on the refined reciprocal lattice a filtered image was generated using a 3 × 3 digital mask around each reciprocal lattice point. A one-unit-cell reference area was cross-correlated with the whole filtered image. The positions of the cross-correlation peaks (Fig. 2 *a*) describe distortions from the ideal lattice (Fig. 2 *b*) based on which a smoothed positional correction was applied to AChR in the raw image before Fourier transformation. Fig. 2 *c* shows residual deviations after the application of calculated smoothed distortion to the raw image. The undistorted reciprocal lattice was least-squares refined and the amplitudes and phases were extracted (Henderson et al., 1986). Reflections that appeared beyond the first node of the contrast transfer function (CTF) or of background-corrected amplitudes that were less than the local background were ignored. No CTF correction to the amplitudes were applied. Inverse Fourier synthesis of the amplitude and phase data calculated from nominally untilted images were used to generate projection maps. Averaged projection maps, generated from several different ordered vesicles, were derived by setting one lattice as a standard and scaling the variations in lattice dimensions (always <2.5%) and amplitudes of consistently strong reflections of the rest of the data set accordingly.

Three-dimensional images were reconstructed by combining phase and amplitude for reflections from transforms of various tilted images. The true angle of sample tilt of each image, and the position of the tilt axis for a tilt series, was determined from the alteration in reciprocal lattice spacings (Shaw and Hills, 1981). The data from tilted views were scaled so as to minimize the difference between amplitudes, and the origin position refined so as to minimize phases differences between reflections within a z* interval of 0.003 $Å^{-1}$, found from adjacent samplings of the $F(hkz^*)$. Scaling and phase origin refinement began by comparison with the averaged untilted image. Fig. 3 shows the extent and distribution of tilted data for both the native and the stripped receptor crystals. The discrete values of merged phases and amplitudes for a lattice line were fit to a smooth function by two rounds of nonlinear least-squares fitting of the observations to the transform of a constrained function of finite extent using the protocol of Agard (1983).

Smooth functions for $|F(z^*)|$, and $\varphi(z^*)$ versus z^* were used to initiate refinement. After refinement the smoothly fitted curves were sampled at intervals of 0.0025 $Å^{-1}$ to obtain initial sets of structure factors for the images of native, and of stripped samples. Amplitudes of the stripped set were scaled to those of the native minimizing

$$E = \Sigma_{hkz^*} < F_{nat} >_s - K_{exp}\{-Bs^2\} < F_{str} >_s.$$

The arbitrarily chosen origin in z*, z_0* of the stripped samples was adjusted so as to minimize P, the weighted phase differences between native and stripped data sets.

$$P = \Sigma_{hkz^*} |F_{hkz^*}| \; |(\Phi_{hkz^*,nat} - \Phi_{hkz^*,str} - 2\pi z_0^*)|.$$

Because the phased reflections were to be used in computing a difference map, it was essential to minimize any differences that could arise artificially between spline-fitted data sets during the iterative nonlinear least-squares fitting. Thus, after initial nonlinear least-squares fitting, the entire procedure was restarted for both native and stripped sets, but beginning with a common initial start to the iterations. To generate common starting functions, the scaled and aligned structure factors for both sets were averaged to give

$$F_{av} = 0.5^*(F_{nat} + F_{str})$$

and this averaged set served as the initial function for a final round of fitting to each set of observed three-dimensional data. The final smoothed profiles for some representative lattice lines are shown in Fig. 4 for both the native

Figure 2. (*a*) Positions of the peaks in the cross-correlation map based on the comparison of a reference area to the whole array. Distortions along edges of the lattice are apparent; (*b*) lattice distortions represented as vector displacements (20× actual size) of the centers of gravity of correlation peaks from those based on a perfect lattice; (*c*) residual distortions from exact lattice positions after applying smoothed two-dimensional distortion functions. These distortions are now reduced to <3 Å except at the vertical edges (near the edge of the tubular array).

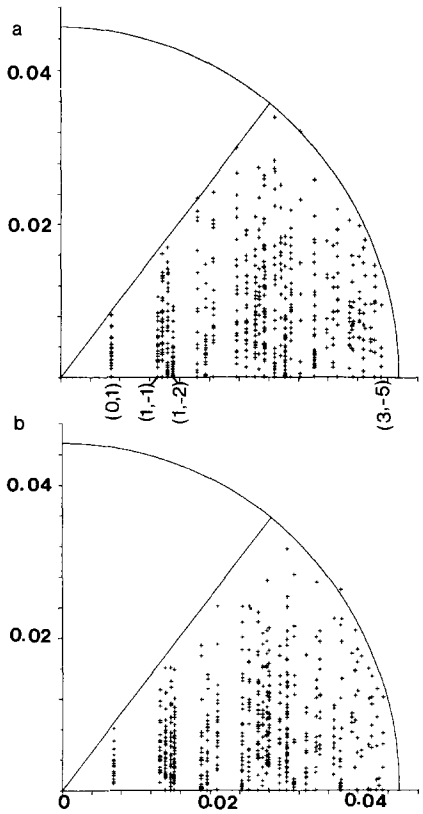

Figure 3. Cylindrically projected distribution of measured three-dimensional data along the lattice lines for (*a*) native and (*b*) alkali-stripped receptor crystals. The ordinate is the reciprocal lattice distance z^* ($Å^{-1}$) normal to the bilayer, the abscissa is the in-plane reciprocal lattice spacing, the circumference indicates 22-Å resolution, and the sector delineates the maximum tilt (52°) at which three-dimensional electron micrographic data were collected in both cases.

and alkaline-stripped AChR. Sampling of the lattice lines, scaling, and phase origin alignment were repeated.

Figures of merit were calculated from the mean values of the cosines of expected error levels in the phases (Fig. 4). Figure of merit weighted amplitudes $m\ |F(z^*)|$ and phases, $\Phi(z^*)$ were inverse Fourier transformed to generate stain-excluding density maps. The expected noise levels $\Delta\rho$ in these maps were calculated using the standard deviation δ of the sampled tilted amplitudes (Fig. 4) and the figures of merit (Dickerson et al., 1968)

$$\Delta\rho^2 = \Sigma_{hkz^*} |F|^2 (1-m^2) + \delta^2.$$

The expected noise level $\Delta\rho$ in the difference map is given as

$$\Delta\rho^2 = \Delta\rho^2_{nat} + \Delta\rho^2_{str}.$$

Data in the Missing Cone Region; Incorporation of X-Ray Data

These purely electron microscopic reconstructions suffer distortions because of the limited tilt angle of ±52°. This elongates all features perpendicular to the membrane (Agard and Stroud, 1982). To compensate partially for this missing cone of data, the contributions along the (00z*) axis, measured by x-ray diffraction were scaled and added in exactly the same fashion to the initial native and alkali-stripped maps to generate hybrid density maps as described below. The electron density profile at 12.5 Å derived from x-ray data we collected from partially oriented stacked AChR membrane preparations (Fairclough et al., 1986) was partitioned into the lipid or non-lipid domains and added in the density domains. Partitioning was according to the measured lipid volume V_{lipid} (Klymkowsky and Stroud, 1979). Thus, the x-ray derived profile $\rho_{total}(z)$ was partitioned to obtain $\rho_{lipid}(z)$ in the lipid region, according to

$$V_{total}\ \rho_{total}\ (z) = V_{lipid}\ \rho_{lipid}\ (z) + (V_{total} - V_{lipid})\ \rho_{total\text{-}lipid}\ (z).$$

The volume assigned to protein within the lipid bilayer implied a radius of the protein in the bilayer region of ~30 Å appropriate for a bundle of 20–25 close packed α-helices (Ross et al., 1977). The x-ray derived density was added as $\rho_{lipid}(z)$ within the volumes of lipid V_{lipid}, and $\rho_{total\text{-}lipid}$ (z) everywhere else. The lipid and protein densities were added to the initial density map in real space. The edges of the bilayer region where there are abrupt loss of contrast in the stain-excluding density map served to align the profile density. The F (00z*) were scaled to the electron micrographic data such that after inclusion the lipid head group density was 0.45 e/$Å^3$, where the protein was 0.44 e/$Å^3$ (Ross et al., 1977).

To locate ordered associated components in the native reconstruction, a difference stain-exclusion map was synthesized. Computed in real space, this was a native-minus-stripped difference density map. The treatment with base altered the stain accessibility within what should be constant regions of the protein (see Discussion) and therefore resulted in additional pairs of positive–negative difference peaks associated with disordering rather than removal of ordered components. To distinguish features resulting from removal of protein rather than disordering, a difference map showing those differences that were positive (stain excluding) in the native structure, and zero or below indicating high stain accessibility in the stripped was used to identify components, like the 43-kD protein, that had been removed.

Results

The stain-exclusion density maps were reconstructed from images of 6,600 AChR molecules averaged in the cumulative tilt series for native and 7,100 for alkaline-stripped AChR arrays.

Crystal Formation Is Stable, and not Induced by Proteolysis

Soon after preparation, native AChR vesicle suspensions are characteristically globular (Fig. 5). Ordered helical arrays of AChR in tubular structures appear spontaneously, in native membrane vesicles prepared from *T. californica* upon incubation at 2°C (Fig. 6, *a* and *b*). These arrays are well ordered, with diffraction apparent out to 22 Å (Fig. 1, *a* and *b*). The time it takes for the ordered vesicles to appear varies between preparations, from as early as 9 d after vesicle preparation to as long as six mo. After their appearance, however, ordered vesicles persist apparently indefinitely, as demonstrated in Fig. 6 *c*, provided the sample solution is kept free from proteases and bacterial contamination. Examination of the ordered vesicle solutions by SDS gel electrophoresis, as shown in Fig. 7 (lanes *b–e*) confirms that the samples were kept protease and bacteria free. Thus, proteolysis of the AChR is not the driving force behind ordered vesicle formation.

Clustering and Lattice Formation Does not Require 43-kD or Associated Proteins

After complete removal of extrinsic membrane proteins from the sample by alkaline extraction, the vesicles in the AChR suspension are dramatically changed in morphology, typically smaller in diameter than the native AChR vesicles and frequently twisted or coiled (Fig. 8). However, spontaneous formation of well-ordered (Fig. 1 *c*) tubes from alkaline-stripped AChR vesicle suspensions is still retained, as indicated in Fig. 9. Also there is no evidence of proteolysis occurring with time during crystal growth (Fig. 7, lanes *d–e*), because of protection by protease inhibitors and bactericidal agents. AChR is typically ~10% of the total protein in native membrane preparations, as the native membrane contains most of the intrinsic and extrinsic membrane proteins of the endplate of *Torpedo* electroplax. However, after removal of extrinsic membrane proteins by alkaline extraction, the AChR

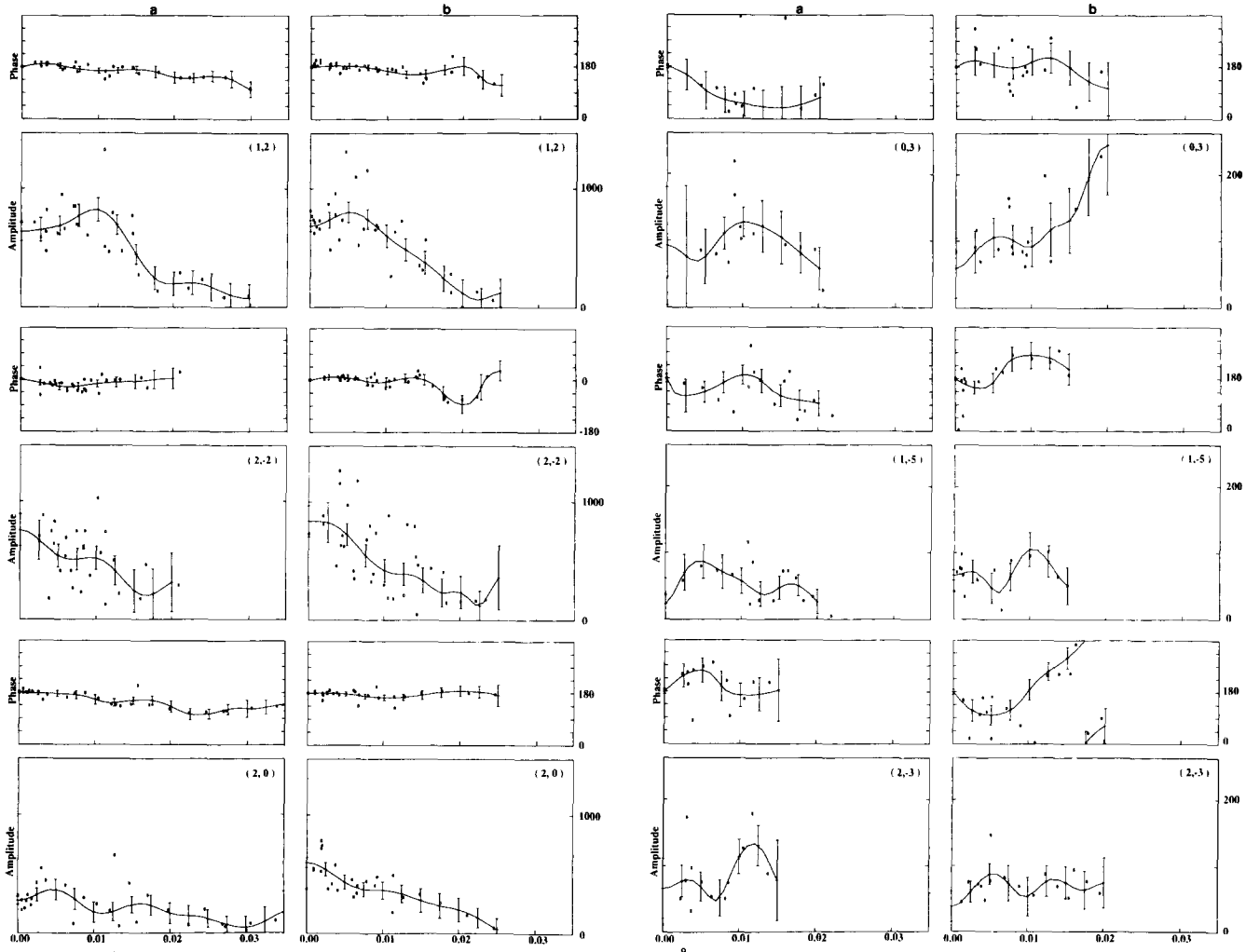

Figure 4. Phase (in degrees) and amplitude variations as a function of z^* ($Å^{-1}$) along several representative (*hkz**) lattice lines for the native (*a*) and the alkali-stripped (*b*) AChR tubes. The curves shown are constrained to the symmetry of the oblique plane group p2 and were obtained by a constrained least-squares fitting procedure (Agard, 1983) (see Materials and Methods). The vertical bars at the sampled positions (0.0025 $Å^{-1}$ = 1/400 $Å^{-1}$ apart) represent estimated error levels after the least-squares refinement.

makes up ~60–65% of the total protein. If subsequently run over an AChR affinity column and eluted with agonist, the AChR from either of the preparations are composed solely of the four subunits of the AChR.

Disulfide Bonded Dimers of AChR Are not Required for Maintenance of the p2 Lattice

The AChR in these vesicle suspensions are largely dimeric, showing the usual ratio of ~80% of AChR as dimer, 20% as monomer (Fig. 10 *c*). Production of entirely monomeric AChR by reduction of the disulfide bond between the δ-subunits with 2 mM DTT does not disorder the two-dimensional arrays of AChR observed in these vesicles, even after incubation in DTT for 24 h at 22°C. An electron micrograph of an ordered AChR vesicle and its computed diffraction pattern, maintained in the presence of reducing agents are shown in Fig. 10, *a* and *b*. Gel profiles of the reduced AChR shown in Fig. 10 *c* clearly demonstrate that the disulfide bond between the δ subunits is broken. This is contrary to the findings of Brisson and Unwin (1984) who observed that the receptor arrays in the tubes from *T. marmorata* become disordered upon reduction.

Specific Activity of AChR Remains during Clustering and Lattice Formation

In our native membrane preparations, the degree of α-BgTx binding does not change with time. α-BgTx binds to affinity-purified (100% pure) AChR with a stoichiometry of 7.5 nM α-BgTx bound/mg AChR. Values for α-BgTx binding to native membrane AChR vesicle suspensions typically ranged from 8–12% (0.79 ± 0.18 nmol α-BgTx bound/mg protein) of that expected for 100% pure AChR, in agreement with the extent of AChR purity observed in the SDS gel profiles. This value did not change from the time of vesicle preparation to after 6 mo of incubation for crystal growth. Thus, there is no gross rearrangement in AChR structure between the time of sample preparation and the appearance of ordered AChR vesicles. The preparations of AChR vesicles after alkaline stripping are 60–65% pure (4.7 ± 0.20 nmol α-BgTx bound/mg protein). However, the alkaline extracted vesicles did not maintain this high level of α-BgTx binding indefinitely, and, 6 mo after preparation, the levels of α-BgTx binding had dropped appreciably (0.86 nmol α-BgTx bound/mg protein). For the purpose of image analysis, no alkaline extracted AChR vesicle suspensions were used more than 4 mo after their preparation.

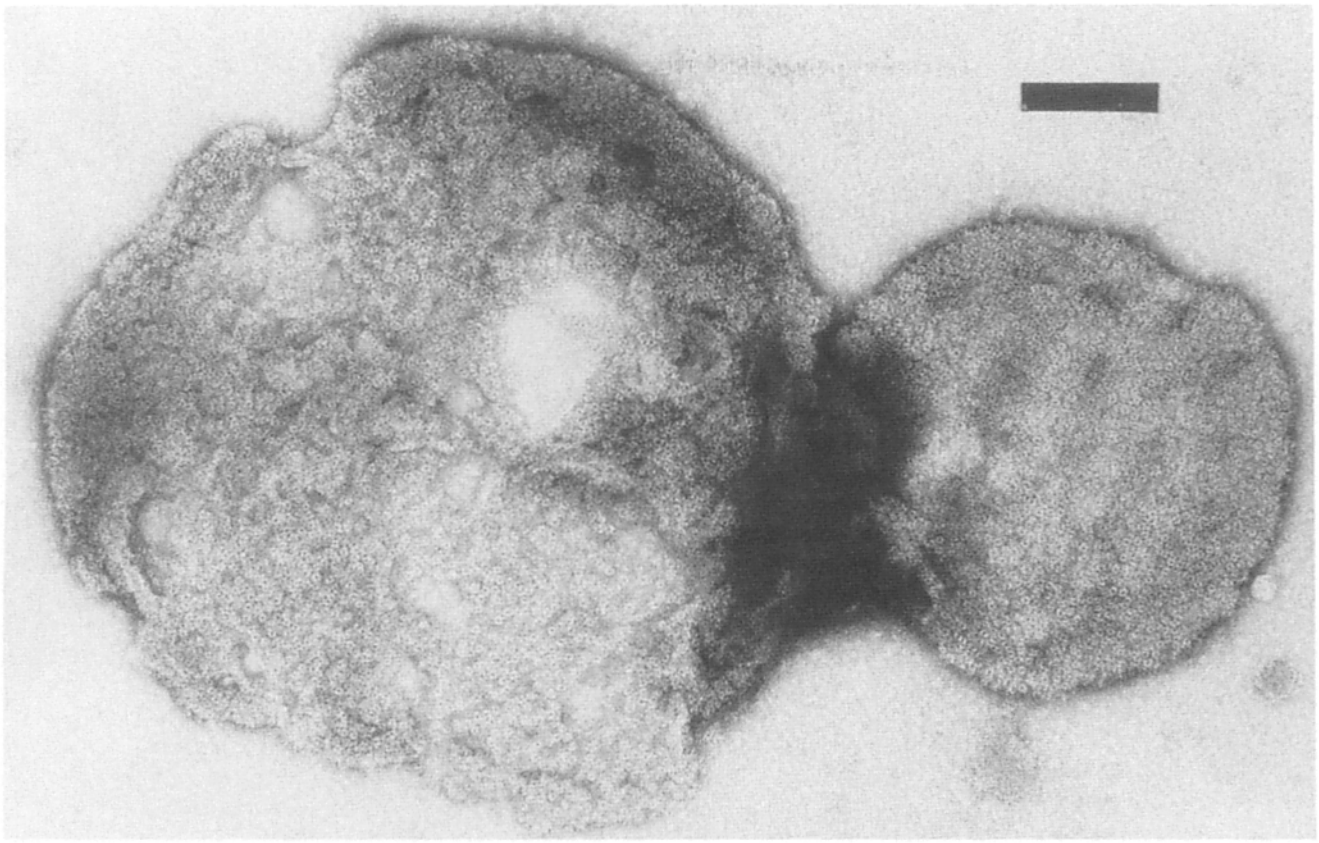

Figure 5. Native AChR vesicles suspension soon after preparation. AChR in these vesicles are close packed, but not crystalline. Samples were prepared as described in Materials and Methods, stained with uranyl acetate, and photographed at a magnification of 40,540. Bar, 0.1 μm.

Carbamylcholine and Toxin Binding to the Latticed AChR

Relatively short term incubation with α-BgTx does not disorder the crystalline vesicles. However, upon long term exposure to α-BgTx (>1 h), arrays of AChR become disordered. This is consistent with the large conformational changes that occur upon complexation (McCarthy and Stroud, 1989*a*). Addition of the agonist carbamylcholine does not disrupt the ordered arrays of AChR. Under these conditions of equilibrium binding, addition of carbamylcholine should desensitize the AChR. The fact that addition of carbamylcholine does not disorder the crystalline arrays of AChR is consistent with our finding that the conformational change(s) associated with desensitization is small, as established by tritium-hydrogen exchange (McCarthy and Stroud, 1989*a*).

The Pentameric Arrangement of Subunits

The presence of weak reflections for k_{odd} indicates that the unit cell contains two molecules. The amplitude-weighted average phase distributions from values of 0° or 180°, after merging of data from six nominally untilted views each for native and stripped tubes, were ±9.0°, and 10.9° respectively, establishing the plane group p2, and the errors in phases (Table 1). This implies a two-fold symmetric arrangement of molecules. The error level in density is 0.5 contours on the scale of Fig. 11 which shows views projected onto the membrane plane. Both forms show the 25-Å-wide vestibular entry to the central ion channel as well as a pentameric arrangement of density peaks separated by 72° ± 3° locating the five quasi-symmetric subunits of the AChR. The ±25% variation in extramembrane stain-excluding volumes of the major peaks around the crest in the projected image, and the peak heights seen in the three-dimensional reconstruction, reflect the different sizes of the five subunits, which differ in mass in the extracellular region by 30%, based on their amino acid sequence (Stroud and Finer-Moore, 1984) and the recently sequenced polysaccharides (Poulter et al. 1989). The five-fold character is more apparent after removal of cytoskeletal and other associated proteins by alkaline-stripping, as depicted in projection in Fig. 11 but dispositions of the major peaks of density, presumed to represent the individual subunits of the AChR, are similar.

In the three-dimensional structure the maximum outer diameter is 74–81 Å. The diameter of the central pore is 24.4 Å for native, and 25.8 Å for alkaline-stripped AChR. Across the pore, the distances between nonadjacent density peaks, presumably representing individual subunits, vary from 44.1–47.8 Å in stripped AChR (Fig. 11). In projection onto the membrane plane the outer diameter of the molecules appear smaller because of the superposition, and are seen as 67.1 Å minimum and 67.7 Å maximum for native AChR and 67.7 Å minimum and 68.7 Å maximum for alkali-stripped AChR.

AChR Lattices Have 20% Less Volume of Lipid than Those Previously Characterized

The unit cell a = 77.7 Å, b = 163.6 Å, γ = 114.9, of area 11,523 Å^2 represents a 10.1% reduction in unit cell area per

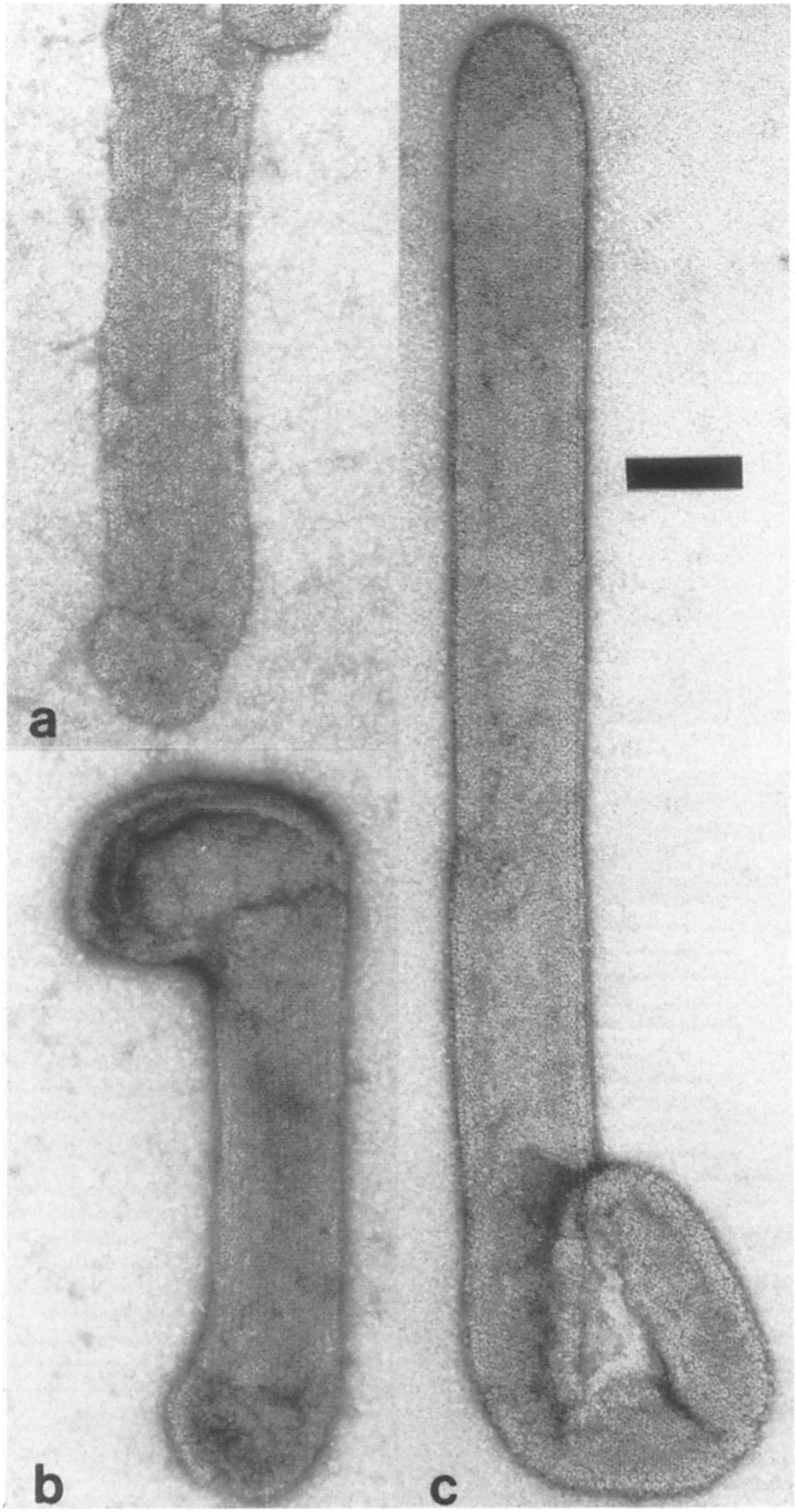

Figure 6. Ordered arrays of AChR in native vesicles persist with time. Electron micrographs of uranyl acetate stained tubular crystals of the AChR, photographed at a magnification of 40,540, are shown after various time intervals of incubation. *a* and *b*, ordered vesicle 2 mo after preparation of incubation solution; *c*, ordered vesicle 11 mo after preparation of incubation solution. Bar, 0.1 μm.

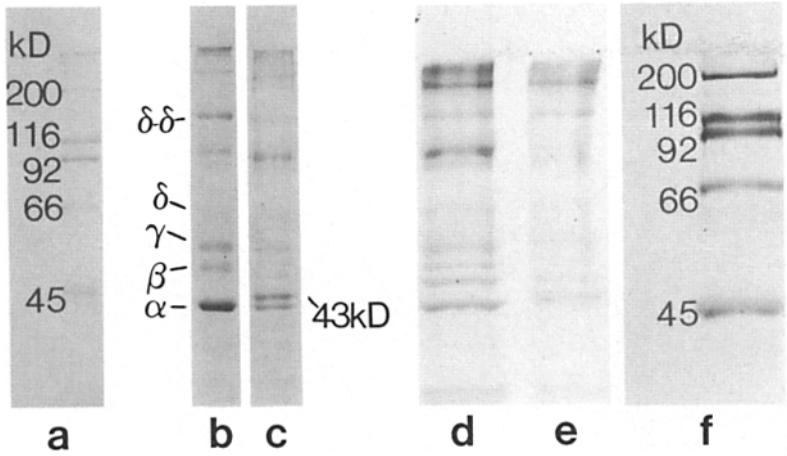

Figure 7. 0.1% SDS/10% acrylamide gels of AChR-containing membranes. Lane *a*, molecular mass standards for lanes *b* and *c*. Lane *b*, positions of the four AChR subunits revealed from an alkali-stripped tube-containing preparation subsequently run on a sucrose-density gradient, lane *c*, native AChR-containing membranes at time zero with the band corresponding to the 43-kD protein marked. Lanes *d–e*, alkaline-stripped AChR-containing membranes at time zero and after 10 mo respectively; lane *f*, molecular mass standards for lanes *d* and *e*.

molecule with respect to that first described by Kistler and Stroud (1981) for native *T. californica* AChR, and a similar 11.1% reduction from the area reported by Brisson and Unwin (1985) and Unwin et al. (1988) for *T. marmorata*. Thus, the packing is tighter than that observed in the tubes of native AChR obtained from *T. marmorata* or those obtained earlier by us from *T. californica*. Since the protein molecules are of the same size, there is thus 20% less volume of lipid in the present lattices.

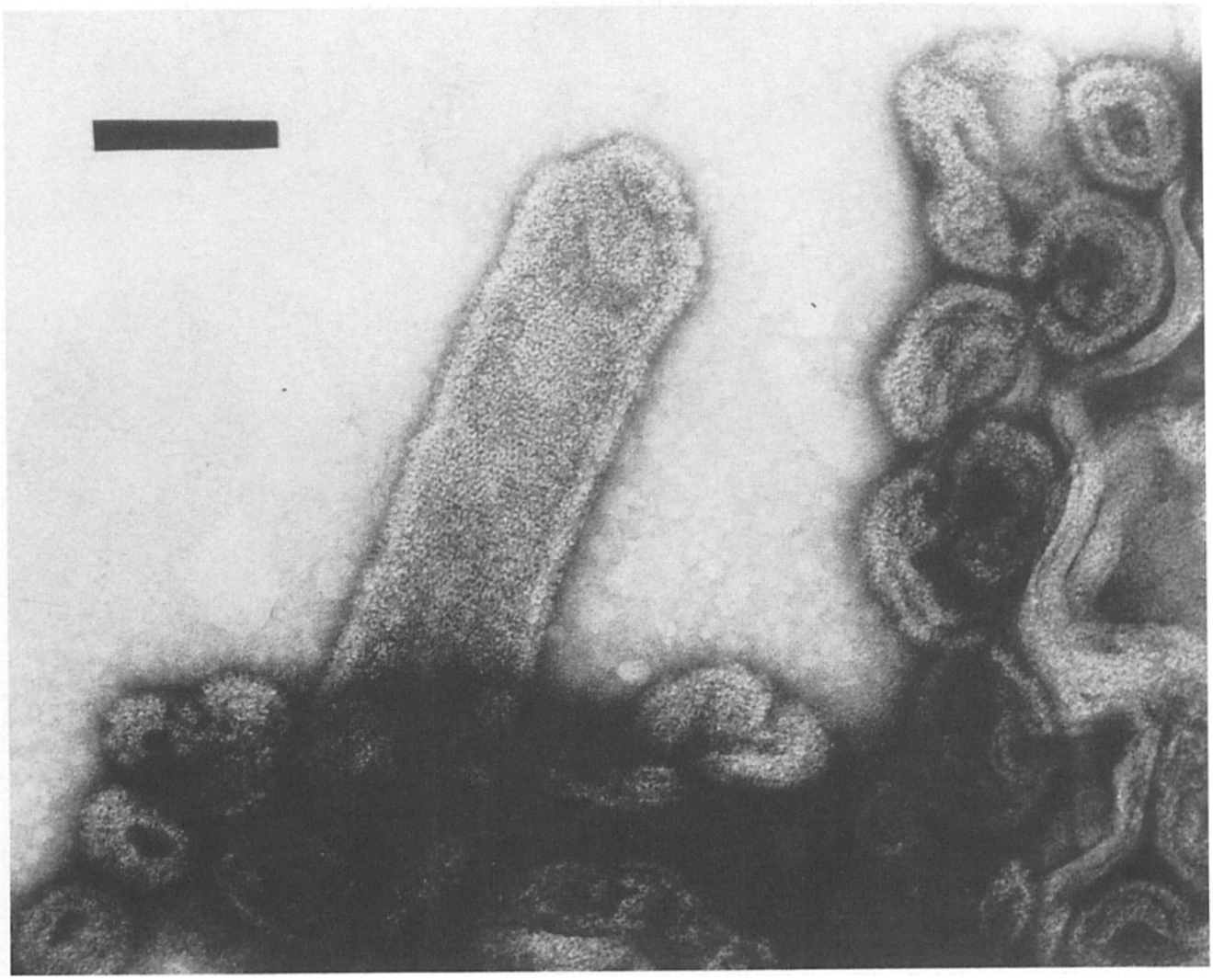

Figure 8. Alkaline-stripped AChR vesicles suspension soon after preparation. AChR in these vesicles are tightly packed, but not crystalline, stained with uranyl acetate, and photographed at a magnification of 85,900. Bar, 0.1 μm.

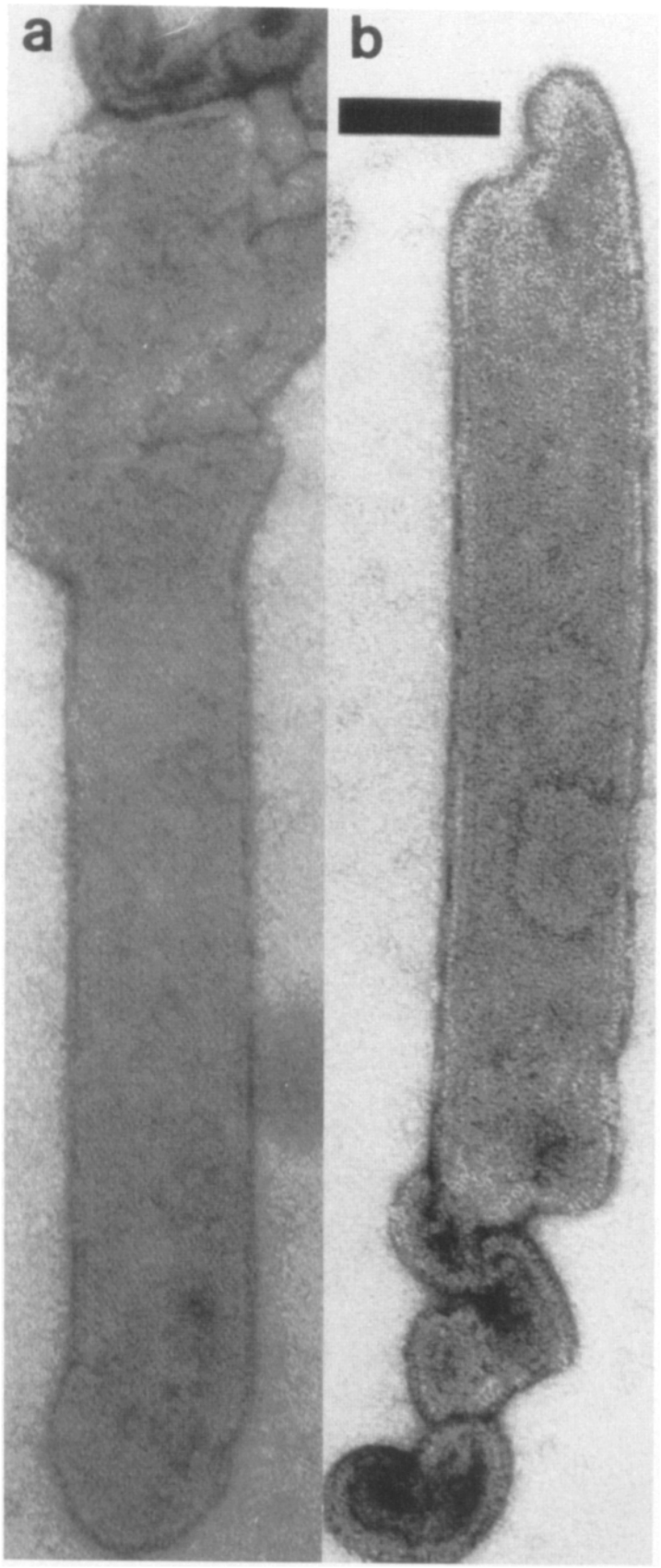

Figure 9. Ordered arrays of AChR in alkaline-stripped vesicles. Electron micrographs of two uranyl acetate stained tubular crystals of the AChR, photographed at a magnification of 40,540, are shown. Bar, 0.1 μm.

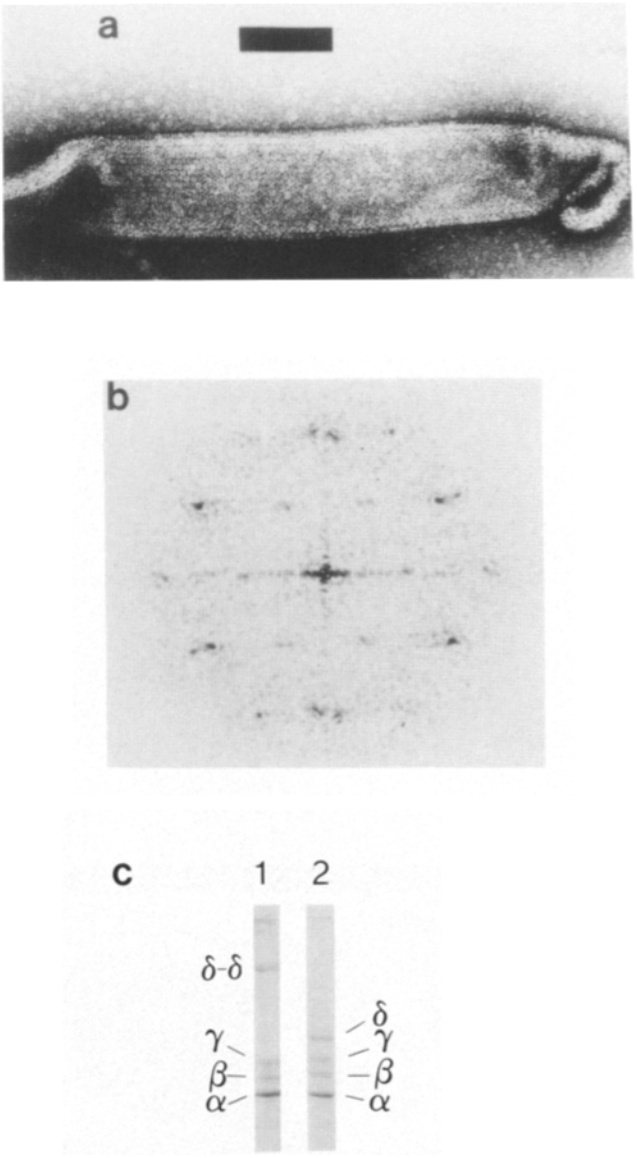

Figure 10. Effects of reduction of disulfide bonds on the AChR and its ordered arrays are revealed by SDS-PAGE and in morphology. Vesicle solution containing ordered arrays of AChR was incubated with 2 mM DTT at 22°C for 1 h. (*a*) Ordered arrays of AChR imaged at a magnification of 40,540. (*b*) Computed diffraction pattern of a well-ordered region from *a*. (*c*) 0.1% SDS/10% acrylamide gels of aliquots of the reduced vesicle solution, and nonreduced AChR vesicle solutions are shown. Lane *1*, native AChR tube containing sample, incubated at room temperature with no DTT; Lane *2*, native AChR tube containing sample incubated at room temperature with 2 mM DTT. The appearance of the δ–δ dimer in the unreduced sample, and δ-monomer after reduction of the AChR, respectively, is indicated.

Three-Dimensional Structure of AChR

The cylindrical infundibular shape of AChR, reflecting directly a key aspect of its function, is apparent in the three-dimensional reconstructions of AChR structure, shown as stereoscopic views from the synaptic side and normal to the bilayer both in the presence (Fig. 12 *a*) and absence (Fig. 12 *b*), of cytoskeletal cross-linking and other associated proteins. The entry well is 25 Å wide and 54 Å deep, and it is surrounded by a protein wall 24.5 ± 1.5-Å thick. The widest outer diameter of the structure is 81 Å, 38 Å above the phosphatidyl head groups. The total length of the complex is 115 Å (Fig. 13 *a*). After alkali-stripping the infundibular protein domain is more extended at 62 Å above the membrane, and the entire AChR is 130 Å long (Fig. 13 *b*); the density appears more dispersed at the top and bottom which is probably because of the disordering effect of the treatment at pH 11.0, though the in-plane diameter of 72 ± 2 Å is unchanged.

The extra-cellular volume of the receptor protein density is ~215,000 Å^3 in the alkaline-stripped form. This volume corresponds to a molecular mass of 167 kD, calculated using the partial specific volume of 0.78 cc/gm (Popot and Changeux, 1984). Columns of density, almost certainly corresponding to the individual subunits, descend slightly inclined to the vertical axis through the AChR, each acting as one, near vertical stave around the central channel (Kistler et al., 1982; Stroud and Finer-Moore, 1985; Brisson and Unwin, 1985).

After alkali-stripping which removes a significant amount of stain excluding mass, the volume of stain excluding material in the cytoplasmic domain lies approximately in a cylinder of radius 33.5 Å, thickness 23 Å for a volume of 81,000 Å, equivalent to that expected for 62 kD of protein. This agrees with calculated cytoplasmic domain predicted on the

Table I. Averaged Projection Structure Factors with Estimated Error Levels for Native and Alkali-stripped AChR Tubes

		Native		Stripped	
h	k	Amplitude	Phase	Amplitude	Phase
0	1	20 (9)	0 (43)	–	–
0	2	543 (112)	180 (13)	456 (109)	180 (8)
0	3	44 (6)	180 (24)	77 (2)	180 (40)
0	4	601 (136)	180 (7)	476 (173)	180 (5)
0	5	28 (22)	180 (23)	–	–
0	6	–	–	62 (31)	180 (30)
1	−6	59 (15)	0 (22)	82 (15)	0 (18)
1	−5	37 (15)	180 (34)	39 (4)	180 (44)
1	−4	746 (73)	0 (9)	715 (164)	0 (8)
1	−3	–	–	39 (28)	0 (28)
1	−2	230 (85)	0 (9)	272 (93)	0 (10)
1	−1	53 (36)	180 (21)	–	–
1	0	364 (145)	180 (9)	299 (95)	180 (11)
1	1	39 (7)	0 (39)	29 (3)	180 (32)
1	2	715 (83)	180 (3)	747 (186)	180 (3)
1	5	15 (4)	180 (30)	18 (16)	0 (34)
2	−5	6 (4)	0 (35)	39 (27)	0 (9)
2	−4	281 (100)	180 (10)	259 (101)	180 (6)
2	−3	11 (7)	180 (3)	–	–
2	−2	705 (162)	0 (5)	668 (195)	0 (8)
2	0	318 (73)	180 (10)	344 (102)	180 (18)
2	1	24 (9)	0 (6)	52 (19)	0 (28)
2	2	–	–	84 (2)	180 (46)
3	−5	56 (24)	0 (6)	123 (27)	0 (3)
3	−2	30 (8)	180 (8)	48 (25)	0 (34)
3	−1	12 (9)	180 (11)	82 (13)	180 (39)
3	0	33 (20)	0 (17)	–	–

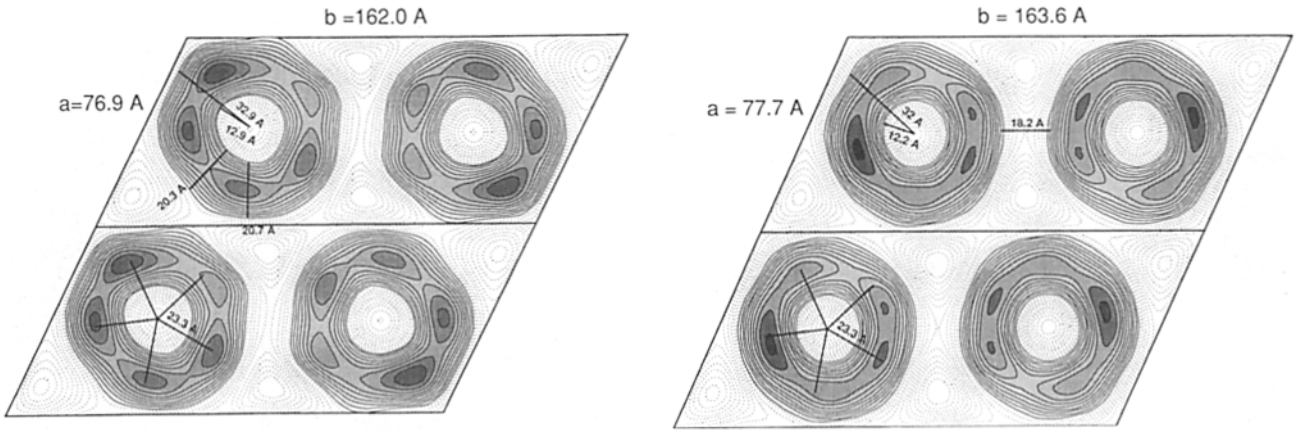

Figure 11. Filtered projection images of (*a*) native and (*b*) alkaline-stripped AChR. The subunit arrangement $\alpha\beta\alpha\gamma\delta$ viewed from the synaptic side of AChR was first determined by Kistler et al., 1982, Fairclough et al., 1983, and later supported for *T. marmarota* also by Unwin et al., 1988. The pentameric nature of the structure is apparent in both cases, but more so after removal of peripheral proteins in b. Solid line contours correspond to the stain-excluding protein portion of the reconstruction, and the dotted lines indicate the stain-binding, non-proteinaceous regions of the map. The unit cell dimensions for the native AChR are a = 77.7 (±2.0) Å, b = 163.6 (±4.0) Å, included angle γ = 114.9 (±2.5)°, and for the alkaline-stripped form are a = 76.9 (±2.0) Å, b = 162.0 (±3.2) Å, included angle γ = 116.0 (±1.8)°.

basis of the four crossing (76-kD) or five crossing (59-kD) models. On the cytoplasmic side, the density contours are always lower than in the ordered extracellular entry well, indicating a less ordered structure on this side that is more permeated by stain. This is true in frozen hydrated images also (Brisson and Unwin, 1985).

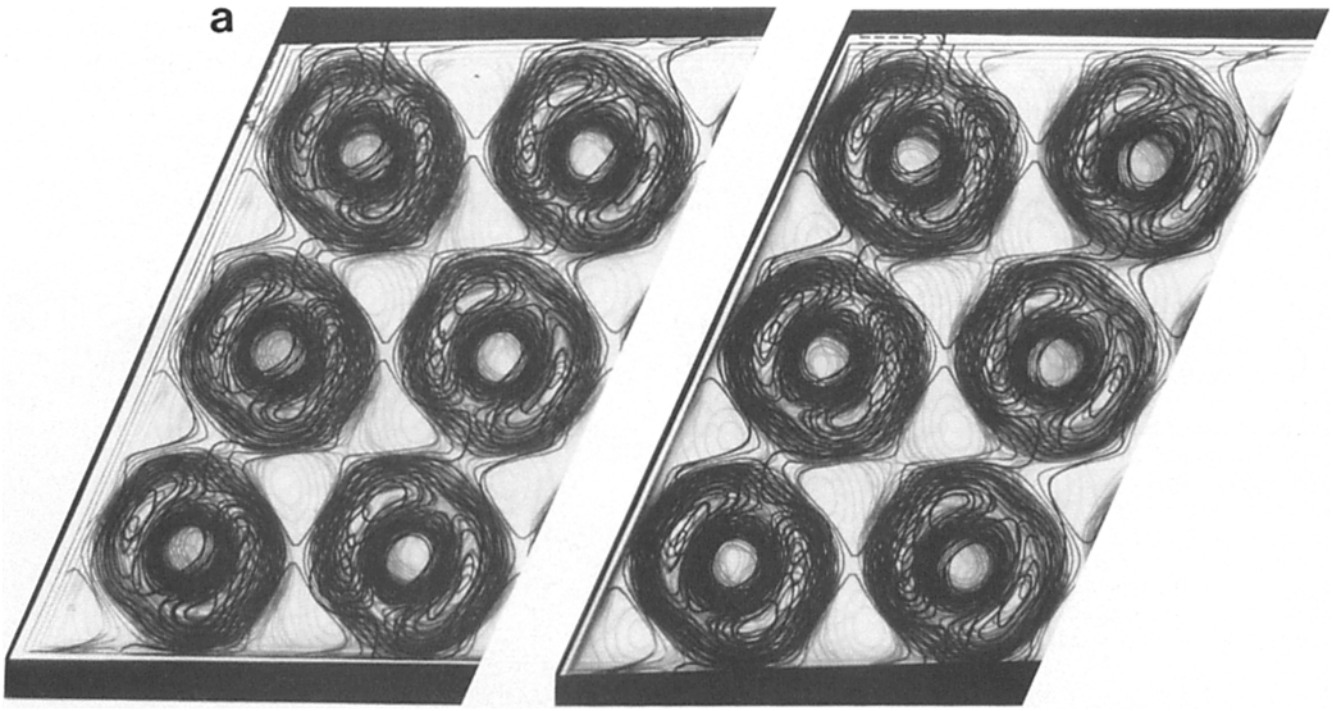

Figure 12. (*a*) Three-dimensional structure of native AChR with the 43-kD protein bound, viewed from the synaptic side at 22-Å resolution. A crossed-eye stereo pair for a 130-Å-thick slab of the hybrid reconstruction made up of sections 10 Å apart are shown. Only positive density contours enclosing protein regions or lipid head groups at the bilayer extremities are indicated. (*b*) Three-dimensional structure of alkaline-stripped AChR after the removal of associated proteins most notably the cytoskeletal 43-kD protein as seen at 22-Å resolution and viewed from the synaptic side. This figure was generated as in a. The electron microscopic tilt data up to 22-Å resolution included those from the significant lattice lines (0, 1), (0, 2), (0, 3), (0, 4), (0, 5), (1, −6), (1, −5), (1, −4), (1, −3), (1, −2), (1, −1), (1, 0), (1, 1), (1, 2), (1, 3), (1, 4), (2, −5), (2, −4), (2, −3), (2, −2), (2, 0), (2, 1), (2, 2), (3, −2) and (3, 0) for the native and (0, 1), (0, 2), (0, 3), (0, 4), (0, 5), (0, 6), (1, −5), (1, −4), (1, −3), (1, −2), (1, −1), (1, 0), (1, 1), (1, 2), (1, 4), (1, 5), (2, −5), (2, −4), (2, −3), (2 −2), (2, −1), (2, 0), (2, 1), (2, 2), (3, −3), (3, −1), and (3, 0) for the alkali-stripped tubes.

The 43-kD Actin-binding Protein Lies below the Bilayer not the AChR, and Contacts the Cytoplasmic Surfaces of Subunits in AChR

A stain-excluding volume of density apparent on the cytoplasmic side extends down 27 Å below the membrane surface in the presence of cytoskeletal and associated proteins, and it is not evident in the reconstruction calculated in the absence of these proteins. This density, which is reproducibly ~4 times the noise level in the maps, appears between and beneath adjacent AChR monomers, and is revealed in a difference stain-exclusion map of native minus alkaline-stripped forms of the AChR (Fig. 13 *c* and 14). The volume of this main density peak is 28,000 $Å^3$, which corresponds to a molecular mass of ~22,000 D. The density in this stain excluding volume is 30% of that in the highest density region on the synaptic side suggesting either some disorder or incomplete occupancy of the 43-kD protein. The position, approximate size and 1:1 stoichiometry with the AChR suggests that this density represents the location of the 43-kD protein, the cytoskeletal cross-linker. In Fig. 14 the cytoplasmic apposition of this density relative to the receptor molecule is shown as viewed normal to the bilayer.

Discussion

This is the only structural analysis of the five subunit AChR where the 43-kD cytoplasmic protein normally present at a 1:1 stoichiometry with AChR, and the other minor associated proteins were removed from the sample before crystallization, confirmed by SDS-PAGE. Comparison with the native AChR structure, therefore, should provide the most reliable picture of what constitutes the minimal five subunit AChR, and define the location of the 43-kD protein.

Formation of Latticed AChR Does not Depend on 43-kD Protein or on Proteolysis; It Requires AChR–AChR Forces, and May Depend on Alterations in the Lipids

Crystalline arrays form within the same time frame, after removal of the 43-kD and most other peripheral proteins, as when they are present demonstrating that 43-kD protein is not required for lattice formation. This then raises the question of how clustering in the cell is accomplished. The arrays observed in vitro reflect some inherent AChR–AChR affinity that may assist in the much more rapid recruitment and close packing, almost as close as seen in the arrays here, at the motor endplate in vivo (Matthews-Bellinger and Salpeter, 1978). The packing is visualized in vivo in rapidly frozen tissue by Heuser and Salpeter (1979). The 43-kD protein and actin may affect the rate and location of clustering in vivo. However, since the energy minimum state in membranes without 43-kD protein seems to lie in latticed close packing of AChR, we consider what other forces could lead to lattice formation in vitro.

In vitro, ordered arrays of membrane-bound AChR from *T. californica* occur spontaneously in sheets (rare) (Ross et al., 1977), and in tubes, first described and characterized by Kistler and Stroud (1981). Tube formation was later observed for AChR from *T. marmorata* (Brisson and Unwin, 1984, 1985), where ordering was better than found by Kistler and Stroud (1981). By leaving out contact with sucrose (the sucrose density gradient step) from the preparations of Kistler and Stroud (1981), and in the presence of protease inhibitors as before, we grew better-ordered tubes from *T. californica* membranes that justified an accurate three-dimensional analysis. In these tube lattices, AChR are 10–15% more close packed in terms of total area of the membrane occupied by protein than in any of the above cases. Thus, the volume of

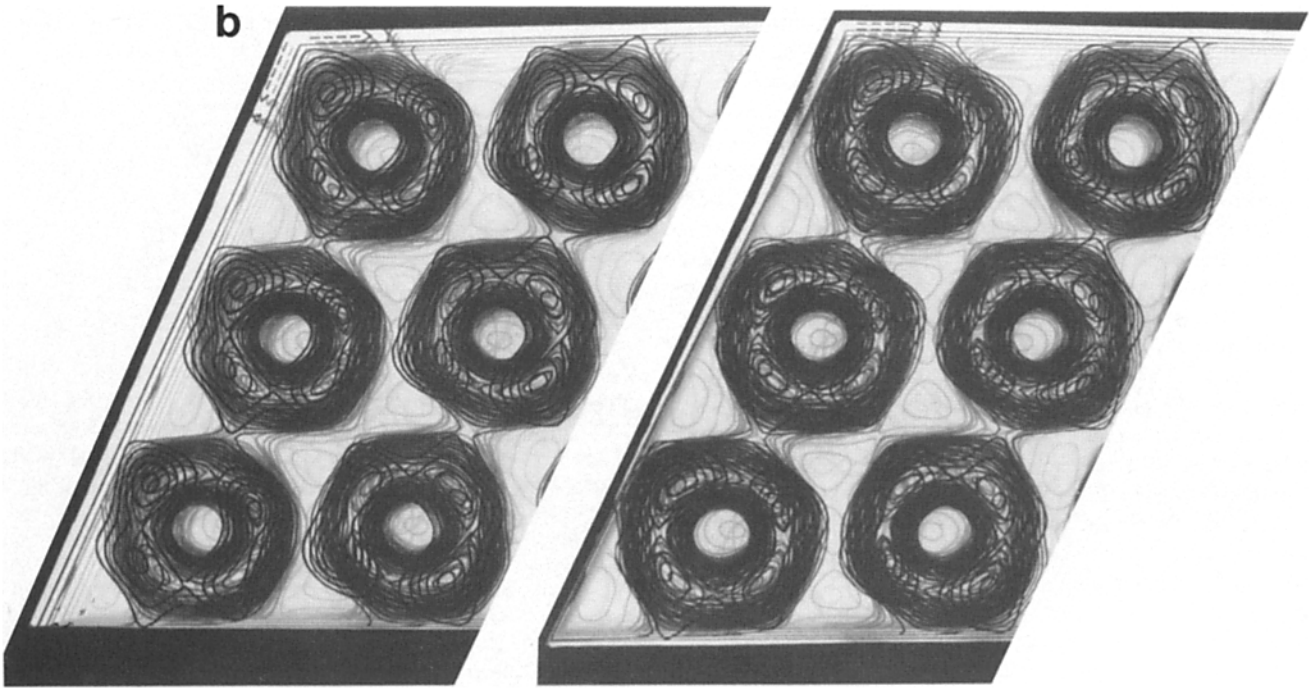

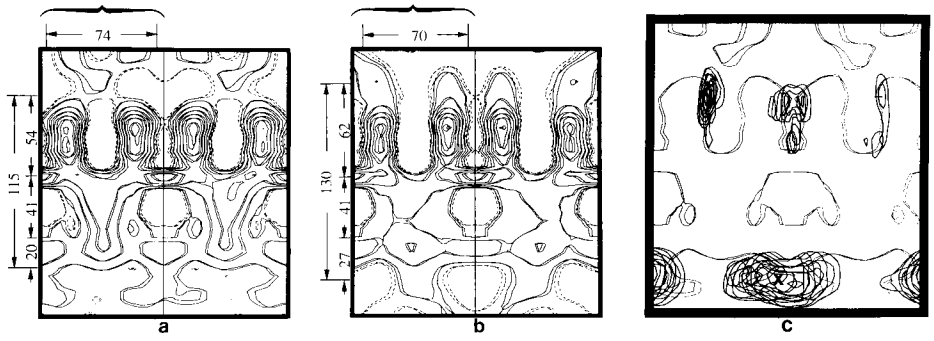

Figure 13. Side view section for a 4-Å slice through the middle of the hybrid AChR reconstructions both in the native (*a*) and alkali-stripped AChR (*b*), and (*c*), a 20 Å slice through the stain exclusion difference map generated by comparing these two forms and superposed on the outline of native AChR shown in a. Only the difference-densities up to the top of the receptor particle are shown in *c*. The major stain-excluding density marked by X represent the putative cytoplasmic location of the 43-kD protein. The horizontal extent of the maps in *a* and *b* are from 0 to *b*, while in *c* it is from $-b/2$ to $b/2$. In *a* and *b* the solid lines enclose proteinaceous regions or lipid head groups at the bilayer extremities, the dashed lines above and below the 41-Å bilayer span delineate stain-binding regions; while within the bilayer these represent the low-density terminal regions of the lipids. The dimensions indicated are in Å.

the lipid content of the unit cell is ~20% smaller though the protein complex is of the same size. This could be because of a facilitation of protein–protein interactions caused by migration of the lipids away from latticed AChR, or because of progressive loss of functional phospholipid, as unsaturated fatty acyl side-chains become oxidized.

The formation of the ordered arrays studied previously (Kistler et al., 1981), or here is not because of proteolysis of the AChR, as evidenced by our SDS polyacrylamide gel analysis of AChR vesicle preparations even 10 mo after incubation in our sterile conditions. Proteolysis by trypsin leads to a different form of AChR aggregation, predominantly in small spherical vesicular particles, though the general morphology of AChR molecules themselves as observed in the electron microscope, or the size as seen on sucrose density gradients is qualitatively remarkably insensitive to limiting tryptic cleavage (Klymkowsky et al., 1980). Likewise, there is qualitatively little obvious difference between the projected images of lattices prepared and incubated in the absence of bacterial inhibitors and incubated in the absence of protease inhibitors in the crystallization solutions (Brisson and Unwin, 1984, 1985), and those with the addition of protease inhibitors to the cyrstallization solutions (Kistler and Stroud, 1981; Kubalek et al., 1987, and this study). Brisson and Unwin (1985) could not visualize the bilayer in micrographs after the 3–4-wk incubations were carried out in Tris buffer, pH 7.5 at 4–17°C in the absence of bacterial or protease inhibitors. Under such conditions, bacterial lipase activity can be a factor. Crystallization of other membrane proteins has been induced by addition of exogenous phospholipases to reduce the amount of competent phospholipid, causing the membrane proteins to associate tightly in the remaining lipid vesicles (Manella, 1984). In our case here, previously (Kistler and Stroud, 1981), and in that of Toyoshima and Unwin (1988) the bilayer is visible in the stain excluding region showing that it is structurally fairly intact, and it is unlikely that lipases induce crystallization.

The ordered AChR vesicles studied here required 50 mM Ca^{2+} for formation, perhaps to depolymerize the cytoskeletal actin network. In the native membrane vesicles, the 43-kD protein was still present, and loss of the actin skeleton may have been required before AChR could freely diffuse in the plane of the bilayer and pack to form an ordered array.

Biochemical analysis of the native ordered AChR vesicles indicate that the AChR in these vesicles are unaltered by the incubation conditions required for crystal growth. There is no significant change in either the gel profiles or the α-BgTx binding behavior of the aged, ordered AChR vesicle solutions relative to freshly prepared native AChR. This is in agreement with the suggestions above that the driving force(s) behind crystal growth is not some change in the protein, but rather crystallization toward a free energy minimum state.

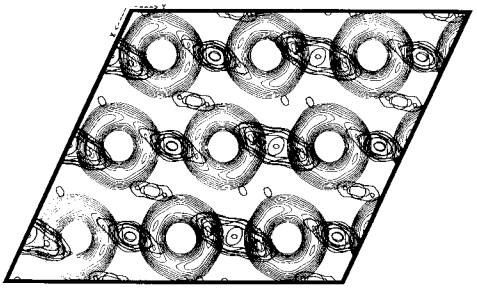

Figure 14. A view normal to the bilayer of the stain-exclusion difference map looking into the cytoplasmic domain. This is a 50-Å slice of sections 10 Å apart. The density marked by X revealed on the cytoplasmic side indicates the density assigned to the 43-kD protein shown apposed against a lighter image of AChR particles in projection. The integrated density of the peak corresponds to 44,000 kD of protein. The other peaks (maximum 10 kD) seen at symmetrically related positions may represent protein, or may have been displaced from the main peak by lower weights for the phases of the weakest reflections (*k* odd), so representing additional density displaced from the main 43-kD protein peak.

The Disulfide Bond between δ Chains Is not Required to Maintain the p2 Lattice

Treatment with DTT at concentrations that reduce all δ–δ disulfide bonds, does not disrupt the ordered arrays, and, therefore, the covalent linkage, which typically cross-links ~80% of δ subunits to make AChR–AChR dimers, is not necessary for maintaining crystallinity. This is contrary to the suggestion of Brisson and Unwin (1984) that this was the basic paring interaction after their finding that small amounts of DTT dispersed lattices of AChR from *T. marmorata*. The two-dimensional crystal form of the AChR we describe here is based on two-fold symmetry as were those studied by Brisson and Unwin (1984, 1985). Thus, the covalent disulfide bond that cross-links congruent residues of the δ chains of AChR is not essential for maintenance of the two-fold symmetry in the lattice. When the mobility of cross-linked dimers of AChR was measured in membranes, we found that the bond was flexible as if on a long disordered chain; the distance between cross-linked dimers varied from 90–120 Å, and the angle varied by ±22° (Fairclough et al., 1983). Only in electric rays are there disulfides between subunits of adjacent AChR complexes, and AChR from other organisms lacks a cysteine at the penultimate residue of the δ chain that is presumed, though not proven, to be the linking residue. Thus, there is no general significance to the covalent dimerization among receptors of this class as regards aggregation during synaptogenesis. Dimers and chains of molecules, as revealed by Heuser and Salpeter (1979) can therefore be maintained by noncovalent AChR–AChR and AChR–43-kD interactions.

Three-Dimensional Structure of AChR: X-Ray Diffraction Removes Distortions of the Electron-Microscopic Analysis

The limited tilt angle of a planar sample results in a distortion of the resulting electron microscopic reconstruction. The primary effect is because of the unobserved region of diffraction around the z* direction (see Fig. 3). This "missing cone" of information in diffraction space produces a false anisotropic extension of structural features perpendicular to the grid; i.e., perpendicular to the bilayer, by a distance about equivalent to the in-plane resolution of the reconstruction (Agard and Stroud, 1982). Strictly, all features in the reconstructed image are convoluted with a prolate ellipsoidal function $\rho(r)$, which is the Fourier transform of the observed volume of the diffraction pattern G(s). $\rho(r)$ has the shape of a prolate ellipsoid of axial ratio ~2.0, and a minor axis diameter about equal to the resolution limit. Because of the convolution with $\rho(r)$, features are falsely elongated perpendicular to the plane of the EM grid (membrane plane) by approximately the resolution limit/2 at both top and bottom; i.e., ~10 Å at the top, and ~10 Å at the bottom. Features that lie parallel to the membrane plane (including the bilayer itself) get diminished in density to the point of relative invisibility by this effect (Agard and Stroud, 1982). The bilayer is therefore not seen directly in the electron micrographic reconstructions though its position, clearly visible in the x-ray diffraction profile, (Ross et al., 1977; Stroud and Agard, 1979) and in side views of AChR vesicles (Klymkowsky and Stroud, 1979; Kistler et al., 1982) can here be localized as the region where contrast between the stain, and the stain-excluding protein is diminished because of the minimal stain penetration into lipids and protein in the bilayer.

The effect of the distortion because of the missing cone can be reduced by deconvolution (Agard and Stroud, 1979), by inclusion in the reconstruction of the transforms of perpendicular views, or by inclusion of x-ray diffraction data. Here we included the perpendicular $F(00z^*)$ terms we had measured by x-ray diffraction (Ross et al., 1977; Fairclough et al., 1986). These correspond to the transform of the electron density perpendicular to the membrane plane. The length of the AChR (perpendicular to the membrane plane) was then seen to be shorter on both the cytoplasmic side and on the outside by 4–6 Å each, with respect to the purely electron micrographic reconstruction. A solid-view representation of this hybrid density map for a pair of AChR in the unit cell is shown in Fig. 15.

The Extracellular Domains of the Infundibulum and Ion Selectivity

The vestibule of the channel has an open diameter of 23 Å reducing to 18 Å diameter close to the level of the phosphatidyl heads on the membrane surface. This diameter must be taken into account in predicting the effects of protein surface charge, of the mostly negatively charged AChR residues, on ionic conductance of the channel. The thickness of the walls varies between 23 and 26 Å. This is typical for the dimensions of antiparallel stranded β barrel structures that are implicated for the extracellular domain of AChR from amphipathic analysis and secondary structure prediction (Finer-Moore and Stroud, 1984; Finer-Moore et al., 1989).

The central channel appears to be ~7 Å in diameter across the narrow transbilayer region, observed by overlapping high resolution images of separated AChR molecules without regard to orientation (Kistler et al., 1982). This is consistent with the sizes of ions that pass through the ion channel (Huang et al., 1978; Dwyer et al., 1980). There is thus a sharp reduction in diameter from 18 to ~7 Å close to the level of the membrane surface. Residues including critical carboxyl groups that affect conductivity, at consensus sequence numbers 280, 284 identified on the basis of mutagenesis (Imoto et al., 1986) lie at the synaptic side of M2; chemical labeling aimed at local anaesthetic binding sites (Hucho et al., 1986; Giraudat et al., 1986; Oberthur et al., 1986; Giraudat et al., 1987) also identify the transmembrane helix that is closest to the channel as M2. The carboxyl residues should then be exposed, solvent accessible, and lie at the floor of the vestibule, at the entrance to the narrowest part of the channel (Fig. 15).

But, in addition, the dipole moment on M2 presents five extra dipolar negative charges, which are expected to lie at a radius of ~9 Å (see Fig. 15) and which may then be exposed within the base of the entry well. These may also serve as key elements in attracting positively charged cations, for which the AChR is specific, to the transbilayer channel.

The transmembrane helices are expected to be 40 Å in length on the basis of sequence (for review, see Stroud and Finer-Moore, 1986), closely matching the measured distance of 41 ± 1 Å between phosphatidyl head groups (Stroud and Agard, 1979). Most probably four (or five) helices per subunit surround the channel for a total of 20 transbilayer helices.

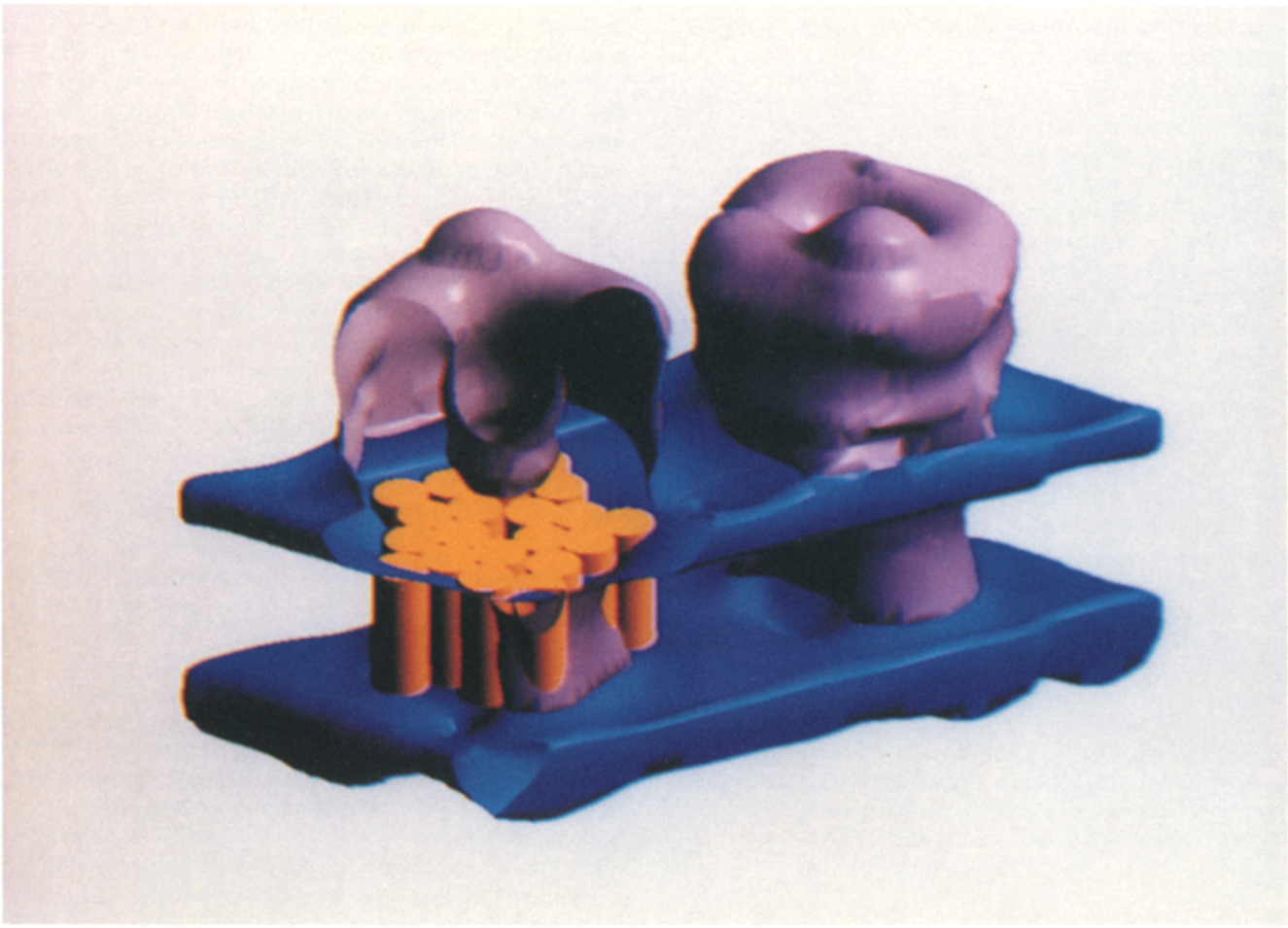

Figure 15. A profile outline of one unit cell of AChR from the three-dimensional hybrid density map of the native structure. The surfaces enclose positive densities. The density for the bilayer, in blue, appears as horizontal planes of densities that correspond to the dense phospholipid head groups that are 41 Å apart. The bundles of cylinders have the dimensions of 30 Å long close-packed α-helices in the center of the bilayer-spanning region, as suggested by x-ray diffraction, and amino acid sequence, and are shown in a cutaway for one of the AChR molecules in the dimer. The figure shows to scale how the closest helices to the channel may lie relative to the entry well. The synaptic side of these helices form the base of the well. The infundibulum extends to just below the surface level of the phospholipid bilayer.

The total length of AChR, seen in the resulting improved density map, is 115 Å in native AChR. It increases after alkali treatment to 130 Å, 8 Å higher above the plane on the synaptic side, and 7 Å larger on the cytoplasmic side that can best be explained as a disordering of the protein domains in response to the treatment at pH 11.0. This redistribution of mass by disordering, visible as increased stain penetration and increased stain excluding volume at the crest, may correlate with the progressive loss of α-BgTx binding after pH 11.0 treatment. Similar disordering may explain the total loss of cytoplasmic density observed by Toyoshima and Unwin (1988), who alkali treated already formed tubular arrays of AChR from *T. marmorata*. Presence of other protein components visible both in the density above the native synaptic surface and on gels of the native membranes may be a factor in preserving order at the crest of the native AChR.

The volume of protein in the density that surrounds the infundibulum on the extracellular side is 215,000 $Å^3$ which corresponds to 167 kD. This is identical to the predicted molecular mass, based on the extracellular portion residues 1–228 of all five glycosylated chains, (Noda et al., 1983, and see Finer-Moore and Stroud, 1984) and the recently determined structures of all oligosaccharide-containing peptides (Poulter et al., 1989) totalling 167–170 kD. The extracellular domains are highly ordered and of well defined structure.

The infundibulum extends 54 Å above the membrane plane in the native membranes; 62 Å after alkaline-stripping. The dimensions of each subunit above the membrane range from 50 to 60 Å in height, by cross section of area 575 $Å^2$ per subunit in the membrane plane. The dimensions of the cross section in the membrane plane are 20 Å radial thickness (as if cut like a pie wedge), by 14 Å in contact with the vestibule by 39 Å of outer circumference. This volume is occupied by the sequence 1–228 in the consensus numbering of Finer-Moore and Stroud (1984) and Stroud and Finer-Moore (1985). Thus, the total contact area between subunits is 1,085 $Å^2$ per interface (vertical, radial cross section of the extracellular portion of the density map), or 2,170 $Å^2$ per subunit. The solvent accessible surface area of the total extracellular region is 18,500 $Å^2$ (3,700 $Å^2$ per subunit), of which ~20%, 3,780 $Å^2$, forms the lining of the infundibulum.

The ion selectivity and conductance of the channel is effected in part by the excess negative charge on the external

regions; this contributes to the selectivity for conducting cations. Negatively charged anions are repelled by the space-charge effect while positively charged cations are attracted to the entry well. 150 negatively charged groups (Glu and Asp) and 98 positively charged lysines and arginines, and 30 histidines are contained in the entire extracellular sequences 1–228 of the five subunits. The isoelectric point calculated for these extracellular regions alone, based on unperturbed pKa values for residues in these sequences is 4.77. The net charge on the extracellular domains expected at pH 7.0 is −50. The average charge density is 1 negative, 0.67 positive charges/25 Å^2 of solvent accessible surface. This represents almost close-packing of charged residues on the AChR surface. Assuming an even distribution of charge, the expected net charge within the entrance to the AChR channel will be an excess of 10 negative charges (30 negatives, 20 positives). It is likely that the outside of the rosette that contacts the negatively charged lipid head groups carries somewhat more positive charge while the inside surface that forms the entry well is more negative. This excessive negative density contributes to the specificity for cation conductivity since electrostatic effects are long range whose effects diminish as $q_1q_2/\epsilon r$.

Dani (1986), Dani and Eisenman (1987) show quantitatively how the effects of the space charge, the surface charge and other factors within an infundibulum of about these dimensions can faithfully generate the observed permeation properties of AChR. The special roles of individual negative charges that are presumably close to the channel entry are illustrated also by site directed mutagenesis (Imoto et al., 1988).

In general, there is little relevant information in the transbilayer region which, though relatively inaccessible, accumulates unevenly a small amount of negative stain. This small stain permeation appears to be more uniform in the alkali-stripped case than in the native and may reflect alterations in the protein information in the bilayer and/or some changes in the lipid organization because of base treatment.

Our three-dimensional reconstructions of the native AChR (with peripheral proteins attached) from *T. californica* in ordered arrays are similar to the three-dimensional structure determinations of AChR from the related species *T. marmorata* (Brisson and Unwin, 1985). The unit cell dimensions give rise to an 11.1% smaller area, the outer diameter in projections (72 Å) and the projection entry diameter (25.5 Å) are similar. Given the differences in biochemistry and staining technique, 2.0% sodium phosphotungstate, or frozen-hydrated (Brisson and Unwin, 1985), 0.2% uranyl-acetate in our case, the extent of agreement is impressive, particularly in the extrasynaptic region, suggesting that the overall structural morphology of the AChR is retained under a variety of conditions. The mouth of the ion channel, an open cylindrical entry funnel, is observed in both reconstructions, as are the indications of the positions of the five subunits, and the relatively disordered and featureless cytoplasmic domain of the AChR.

Other AChR Associated Proteins

Besides 43 kD several other proteins are associated with AChR, some of which are thought to be associated with the formation or stabilization of the junctional specialization. A 58-kD protein that is cytoplasmic has been characterized (Froehner et al., 1987). A 90-kD protein is present at fairly high stoichiometry. A 270-kD protein is present at a stoichiometry of 0.15 mol/mol AChR (Burden et al., 1983). Some stain-excluding density lies above the synaptic crest of the native AChR and is removed in the alkaline-stripped form. This density is probably because of residual elements of the basal lamina on the extracellular side that are known to interact with the AChR (Bayne et al., 1984; Olek et al., 1984). Alkaline treatment of AChR membrane suspensions, removes the many minor AChR-associated proteins seen on the gels (Fig. 7). There is density visible in the difference density maps around the outer crest of AChR. Some of this density is because of a change in ordering of the AChR subunits. No further attempt has been made to interpret the extracellular densities.

The 43-kD Protein Provides an Ordered Linkage between AChR and the Cytoskeleton

The AChR 43-kD protein is concentrated at sites of innervation in the postsynaptic membrane (Peng and Froehner, 1985), and provides for the relative immobilization of the AChR at the synapse (Rousselet et al., 1982). Bridgman et al. (1987) show by freeze-etch and immunoelectron microscopy, that the 43-kD protein is closely associated with AChR, and that the cytoplasmic extension of the AChR-43-kD protein (~50 Å) seems to be on the same scale as the extracellular extension of the AChR.

There is an ordered linkage between AChR and components of the 43-kD protein. The volume of the larger of the two stains excluding features associated with 43-kD protein is ~56,000 Å^3 which corresponds to only 44-kD, or 2 times 22,000 D equivalents of protein associated with each pair of AChR molecules. Thus, only 50% of the 43-kD protein is ordered in a regular latticed array at this site. But the stain excluding density is low, indicating that the sites are only ~35% occupied by the ordered 43-kD protein, or that the 43-kD protein is somewhat variable in conformation. There is a second smaller feature, one half of a unit cell away in the *b* direction, and accounting for 2 times 10 kD of protein. This feature, less than half the mass of the other, may indicate a second type of association with AChR. However, the difference between the two peaks is encoded only in the weakest k = odd reflections that have the greatest phase errors. Thus, another interpretation is that this density should be added to the first one, and that it was only separated because of the phase errors in the weakest reflections.

The cytoplasmic components, both on AChR and the 43-kD protein array, are much less ordered than the outer surface of AChR as seen from lowered contour density, indicating increased stain penetration in those regions. The cytoplasmic domain must also be easily deformed since membranes can fold over one another whereupon phosphatidyl head groups on the cytoplasmic sides of adjacent bilayers are separated by as little as 10–20 Å (Kistler et al., 1982). The sequences of different species of each AChR chains are more variable by a factor of 2 in this domain, again suggesting a less specific role for the less ordered domain (for review, see Stroud and Finer-Moore, 1985 where original sources are referenced for 13 AChR sequences).

In the reconstructed difference images, the 43 kD protein is closely associated with the lipid bilayer as well as with the

cytoplasmic domain of AChR. It binds beside, rather than beneath the AChR. This is consistent with its ability to adhere to liposomes (Porter and Froehner, 1985). There is no strong evidence, biochemical or structural, for a regulatory role as suggested by Toyoshima and Unwin (1988) on the basis of location, nor does there seem to be any major difference in the density that lies underneath the channel where these investigators interpreted 43-kD to lie. There is density there both with and without 43-kD. However, 43-kD and other proteins were not removed from samples in their case, and the brief treatment with base may have only redistributed 43-kD protein on the surface. A danger in both analyses is that diminution of protein volume could be because of disordering rather than removal of protein. There are several regions in our difference map where stain excluding volume becomes more diffuse and less dense, especially around the top crest of AChR (see Fig. 13 *c*). We attempted to avoid this ambiguity by ensuring that the comparison was carried out after complete removal of the 43-kD protein and by selecting those regions of the stain excluding difference map that correspond to significant stain excluding regions in the native (with 43 kD) map but that are completely stain accessible after the removal. This then selects regions in the native structure from which protein is removed.

The subunit closest to the major 43-kD feature (Fig. 14) is probably the β subunit to which it can be most easily cross-linked chemically (Burden et al., 1983).

Quantitative comparison of AChR in presence versus in absence of cytoplasmic components of the AChR shows an ordered association between AChR and cytoplasmic actin-binding components. The projected structure shows a more five-fold symmetric arrangement after removal of the peripheral proteins. However, the AChR pentameric complex itself can aggregate in an ordered fashion that may stabilize the associations at the synapse. The major 43-kD component may be involved in the correct localization of AChR at the synapse, and a major question remains to determine how this occurs.

The high conservation of sequence between AChR from Torpedo, and sequences of neuroreceptors from brain, from the peripheral and central nervous system for acetylcholine (Boulter et al., 1987; Whiting et al., 1987), for γ amino butyric acid (Schofield et al., 1987), and glycine (Grenningloh et al., 1987), imply that consequences the AChR structure has for synaptic transmission will have direct parallels throughout the nervous system.

We thank M. Schmid for use of and discussions of his modifications of lattice unbending software, R. Henderson and D. Agard for use of their programs, H. Chen for use of his program to create three-dimensional solid surfaces used for Fig. 15, and J. Newdoll for preparing Fig. 15.

Research was supported by the National Institutes of Health (GM24485) and by the National Science Foundation (PCM 83 16401).

Received for publication 12 September 1988 and in revised form 5 April 1989.

References

Agard, D. A. 1983. A least-squares method for determining structure factors in three-dimensional tilted-view reconstruction. *J. Mol. Biol.* 167:849–852.

Agard, D. A., and R. M. Stroud. 1982. Linking regions between helices in bacteriorhodopsin revealed. *Biophys. J.* 37:589–602.

Anderson, C. R., and C. F. Stevens. 1973. Voltage-clamps analysis of acetylcholine produced end-plate current fluctuations at frog neuromuscular junctions. *J. Physiol. (Lond.).* 235:655–691.

Barrantes, F. J., D.-Ch. Neugebauer, and H. P. Zingsheim. 1980. Peptide extraction by alkaline treatment is accompanied by rearrangement of the membrane-bound acetylcholine receptor from *Torpedo marmorata*. *FEBS (Fed. Eur. Biochem. Soc.) Lett.* 112:73–78.

Bayne, E. K., M. J. Anderson, and D. M. Fambrough. 1984. Extracellular matrix organization in developing muscle: correlation with acetylcholine receptor aggregates. *J. Cell Biol.* 99:1486–1501.

Bon, F., E. Lebrun, J. Gomel, R. van Rapenbusch, J. Cartaud, J.-L. Popot, and J.-P. Changeux. 1984. Image analysis of the heavy form of the acetylcholine receptor from *Torpedo marmorata*. *J. Mol. Biol.* 176:205–237.

Boulter, J., J. Connolly, E. Deneris, D. Goldman, S. Heinemann, and J. Patrick. 1987. Functional expression of two neuronal nicotinic acetylcholine receptors from cDNA clones identifies a gene family. *Proc. Natl. Acad. Sci. USA.* 84:7763–7767.

Bridgman, P. C., C. Carr, S. E. Pedersen, and J. B. Cohen. 1987. Visualization of the cytoplasmic surface of *Torpedo* postsynaptic membranes by freeze-etch and immunoelectron microscopy. *J. Cell Biol.* 105:1829–1846.

Brisson, A., and P. N. T. Unwin. 1984. Tubular crystals of acetylcholine receptors. *J. Cell Biol.* 99:1202–1211.

Brisson, A., and P. N. T. Unwin. 1985. Quaternary structure of the acetylcholine receptor. *Nature (Lond.).* 315:474–477.

Burden, S. J., R. L. DePalma, and G. S. Gottesman. 1983. Cross-linking of proteins in acetylcholine receptor-rich membranes: association between the β-subunit and the 43 kD subsynaptic protein. *Cell.* 35:687–692.

Cartaud, J., E. L. Benedetti, J. B. Cohen, J.-C. Meunier, and J.-P. Changeux. 1973. Presence of a lattice structure in membrane fragments rich in nicotinic receptor protein from the electric organ of *Torpedo marmorata*. *FEBS (Fed. Eur. Biochem. Soc.) Lett.* 33:109–113.

Cartaud, J., E. L. Benedetti, A. Sobel, and J.-P. Changeux. 1978. A morphological study of the cholinergic receptor protein from *Torpedo marmorata* in its membrane environment and in its detergent-extracted purified form. *J. Cell Sci.* 29:313–337.

Cartaud, J., A. Sobel, A. Rousselet, P. F. Devaux, and J.-P. Changeux. 1981. Consequences of alkaline treatment for the ultra-structure of the acetylcholine receptor-rich membranes from *Torpedo marmorata* electric organ. *J. Cell Biol.* 90:418–426.

Cartaud, J., R. Oswald, G. Clement, and J.-P. Changeux. 1982. Evidence for a skeleton in acetylcholine receptor-rich membranes from *Torpedo marmorata* electric organ. *FEBS (Fed. Eur. Biochem. Soc.) Lett.* 145:250–257.

Conti-Tronconi, B. M., and M. A. Raftery. 1982. The nicotinic cholinergic receptor: correlation of molecular structure with functional properties. *Annu. Rev. Biochem.* 51:491–530.

Dani, J. A. 1986. Ion-channel entrances influence permeation. Net charge, size, shape, and binding considerations. *Biophys. J.* 49:607–618.

Dani, J. A., and G. Eisenman. 1987. Monovalent and divalent cation permeation in acetylcholine receptor channels. Ion transport related to structure. *J. Gen. Physiol.* 89:959–983.

Dickerson, R. E., J. E. Weinzierl, and R. A. Palmer. 1968. A least-squares refinement method for isomorphous replacement. *Acta. Crystallogr. Sect. B Struct. Crystallogr. Cryst. Chem.* 24:997–1003.

Dwyer, T. M., D. J. Adams, and B. Hille. 1980. The permeability of the end-plate channel to organic cations in frog muscle. *J. Gen. Physiol.* 75: 469–492.

Fairclough, R. H., J. Finer-Moore, R. A. Love, D. Kristofferson, P. J. Desmeules, and R. M. Stroud. 1983. Subunit organization and structure of an acetylcholine receptor. *Cold Spring Harbor Symp. Quant. Biol.* 48:9–20.

Fairclough, R. H., R. C. Miake-Lye, R. M. Stroud, K. O. Hodgson, and S. Doniach. 1986. Location of terbium binding sites on acetylcholine receptor-enriched membranes. *J. Mol. Biol.* 189:673–680.

Finer-Moore, J., and R. M. Stroud. 1984. Amphipathic analysis and possible formation of the ionic channel in an acetylcholine receptor. *Proc. Natl. Acad. Sci. USA.* 81:155–159.

Finer-Moore, J., J. F. Bazan, J. Rubin, and R. M. Stroud. 1989. Identification of membrane proteins and soluble protein secondary structural elements, domain structure, and packing arrangements by Fourier-transform amphipathic analysis. *In* Prediction of Protein Structure and the Principles of Protein Conformation. G. Fasman, editor. Plenum Publishing Corp., New York. In press.

Frail, D. E., J. Mudd, V. Shah, C. Carr, J. B. Cohen, and J. P. Merlie. 1987. cDNAs for the postsynaptic 43-kDa protein of *Torpedo* electric organ encode two proteins with different carboxy terminus. *Proc. Natl. Acad. Sci. USA.* 84:6302–6306.

Froehner, S. C. 1986. The role of the postsynaptic cytoskeleton in acetylcholine receptor organization. *Trends Neurosci.* 9:37–44.

Froehner, S. C., A. A. Murnane, M. Tobler, H. B. Peng, and R. Sealock. 1987. A postsynaptic M_r 58,000(58 K) protein concentrated at acetylcholine receptor-rich sites in *Torpedo* electroplaques and skeletal muscle. *J. Cell Biol.* 104:1633–1646.

Froehner, S. C., V. Gulbrandsen, C. Hyman, A. Y. Jeng, R. R. Neubig, and J. B. Cohen. 1981. Immunofluorescence localization at the mammalian neuromuscular junction of the M_r 43,000 protein of *Torpedo* postsynaptic membranes. *Proc. Natl. Acad. Sci. USA.* 78:5230–5234.

Giraudat, J., M. Dennis, T. Heidmann, J.-Y. Chang, and J.-P. Changeux. 1986. Structure of the high affinity binding site for noncompetitive blockers

of the acetylcholine receptor: serine 262 of the δ-subunit is labeled by [^{3}H]-chlorpromazine. *Proc. Natl. Acad. Sci. USA.* 83:2719–2723.

Giraudat, J., M. Dennis, T. Heidmann, P.-Y. Haumont, F. Lederer, and J.-P. Changeux. 1987. Structure of the high-affinity binding site for noncompetitive blockers of the acetylcholine receptor: [^{3}H] chlorpromazine labels homologous residues in the β and δ chains. *Biochemistry.* 26:2410–2418.

Greningloh, G., A. Rienitz, B. Schmitt, C. Methfessel, M. Zensen, K. Beyreuther, E. Gundelfinger, and H. Betz. 1987. The strychnine-binding subunit of the glycine receptor shows homology with nicotinic acetylcholine receptors. *Nature (Lond.).* 328:215–220.

Gysin, R., Wirth, M., and S. D. Flanagan. 1981. Structural heterogeneity and subcellular distribution of the nicotinic synapse-associated proteins. *J. Biol. Chem.* 256:11373–11376.

Gysin, R., B. Yost, and S. D. Flanagan. 1983. Immunochemical and molecular differentiation of 43,000 molecular weight proteins associated with *Torpedo* neuroelectrocyte synapses. *Biochemistry.* 22:5781–5789.

Hayward, S. B., and R. M. Stroud. 1981. Projected structure of purple membrane determined to 3.7 Å resolution by low-temperature electron microscopy. *J. Mol. Biol.* 151:491–517.

Henderson, R., and P. N. T. Unwin. 1975. Three-dimensional model of purple membrane obtained by electron microscopy. *Nature (Lond.).* 257:28–32.

Henderson, R., J. M. Baldwin, K. H. Downing, J. Lepault, and E. Zemlin. 1986. Structure of purple membrane from *Halobacterium halobium*: recording, measurement and evaluation of electron micrographs at 3.5 Å resolution. *Ultramicroscopy.* 19:147–178.

Heuser, J. E., and S. R. Salpeter. 1979. Organization of acetylcholine receptors in quick-frozen, deep-etched and rotary-replicated *Torpedo* postsynaptic membrane. *J. Cell Biol.* 82:150–173.

Holtzman, E., D. Wise, J. Wall, and A. Karlin. 1982. Electron microscopy of complexes of isolated acetylcholine receptor, biotinyl-toxin, and avidin. *Proc. Natl. Acad. Sci. USA.* 79:310–314.

Huang, L.-Y. M., W. A. Catterall, and G. Ehrenstein. 1978. Selectivity of cations and nonelectrolytes for acetylcholine activated channels in cultured muscle cells. *J. Gen Physiol.* 71:397–410.

Hucho, F., W. Oberthur, and F. Lottspeich. 1986. The ion channel of the nicotinic acetylcholine receptor is formed by the homologous helices M II of the receptor subunits. *FEBS (Fed. Eur. Biochem. Soc.) Lett.* 205:137–142.

Imoto, K., C. Methfessel, B. Sakmann, M. Mishina, Y. Mori, T. Konno, K. Fukuda, M. Kurasaki, H. Bujo, Y. Fujita, and S. Numa. 1986. Location of a δ-subunit region determining ion transport through the acetylcholine receptor channel. *Nature (Lond.).* 324:670–674.

Imoto, K., C. Busch, B. Sakmann, M. Mishina, T. Konno, J. Nakai, H. Bujo, Y. Mori, K. Fukuda, and S. Numa. 1988. Rings of negatively charged amino acids determine the acetylcholine receptor channel conductance. *Nature (Lond.).* 335:645–648.

Jackson, M. B. 1984. Spontaneous openings of the acetylcholine receptor channel. *Proc. Natl. Acad. Sci. USA.* 81:3901–3904.

Kistler, J., and R. M. Stroud. 1981. Crystalline arrays of membrane-bound acetylcholine receptor. *Proc. Natl. Acad. Sci. USA.* 78:3678–3682.

Kistler, J., R. M. Stroud, M. W. Klymkowsky, R. A. Lalancette, and R. H. Fairclough. 1982. Structure and function of an acetylcholine receptor. *Biophys. J.* 37:371–383.

Klymkowsky, M. W., and R. M. Stroud. 1979. Immunospecific identification and three-dimensional structure of a membrane-bound acetylcholine receptor from *Torpedo californica. J. Mol. Biol.* 128:319–334.

Klymkowsky, M. W., J. E. Heuser, and R. M. Stroud. 1980. Protease effects on the structure of acetylcholine receptor membranes from *Torpedo californica. J. Cell Biol.* 85:823–838.

Kubalek, E., S. Ralston, J. Lindstrom, and N. Unwin. 1987. Location of subunits within the acetylcholine receptor by electron image analysis of tubular crystals from *Torpedo marmorata. J. Cell Biol.* 105:9–18.

Laemmli, U. K. 1970. Cleavage of structural proteins during the assembly of the head of bacteriophage T4. *Nature (Lond.).* 227:680–685.

LaRochelle, W. J., and S. C. Froehner. 1986. Determination of the tissue distributions and relative concentrations of the postsynaptic 43-kDa protein and acetylcholine receptor in *Torpedo. J. Biol. Chem.* 261:5270–5274.

Lo, M. M. S., P. B. Garland, J. Lamprecht, and E. A. Barnard. 1980. Rotational mobility of the membrane-bound acetylcholine receptor of *Torpedo* electric organ measured by phosphorescence depolarization. *FEBS (Fed. Eur. Biochem. Soc.) Lett.* 111:407–412.

Lowry, O. H., N. J. Rosebrough, A. L. Farr, and R. J. Randall. 1951. Protein measurement with the Folin phenol reagent. *J. Biol. Chem.* 193:265–275.

Mannella, C. A. 1984. Phospholipase-induced crystallization of channels in mitochondrial outer membranes. *Science (Wash. DC).* 224:165–166.

Markwell, M. K., S. M. Hass, L. L. Bieber, and N. E. Tolbert. 1978. A modification of the Lowry procedure to simplify protein determination in membrane and lipoprotein samples. *Anal. Biochem.* 87:206–210.

Matthews-Bellinger, J., and M. M. Salpeter. 1978. Distribution of acetylcholine receptors at frog neuromuscular junctions with a discussion of some physiological implications. *J. Physiol. (Lond.).* 279:197–213.

McCarthy, M. P., and R. M. Stroud. 1989*a*. Conformational states of the nicotinic acetylcholine receptor from *Torpedo californica* induced by the binding of agonists, antagonists and local anesthetics. Equilibrium measurement using tritium-hydrogen exchange. *Biochemistry.* 28:40–48.

McCarthy, M. P., and R. M. Stroud. 1989*b*. Changes in conformation upon agonist binding, and nonequivalent labeling, of the membrane spanning regions of the nicotinic acetylcholine receptor subunits. *J. Biol. Chem.* 264:10911–10916.

McCarthy, M. P., J. P. Earnest, E. F. Young, S. Choe, and R. M. Stroud. 1986. The molecular neurobiology of the nicotinic acetylcholine receptor. *Annu. Rev. Neurosci.* 9:383–413.

Mebs, D., K. Narita, S. Iwanaga, Y. Samejima, and C.-Y. Lee. 1972. Purification, properties and amino acid sequence of α-bungarotoxin from the venom of *Bungarus multienetus. Hoppe-Seyler's. Z. Physiol. Chem.* 353:243–262.

Neher, E., and B. Sakman. 1976. Single-channel currents recorded from membrane of denervated frog muscle fibres. *Nature (Lond.).* 260:779–802.

Neubig, R. R., E. K. Krodel, N. D. Boyd, and J. B. Cohen. 1979. Acetylcholine and local anesthetic binding to *Torpedo* nicotinic postsynaptic membranes after removal of nonreceptor peptides. *Proc. Natl. Acad. Sci. USA.* 76:690–694.

Ngheim, H.-O., J. Cartaud, C. Dubreuil, C. Kordeli, G. Buttin, and J.-P. Changeux. 1983. Production and characterization of a monoclonal antibody directed against the 43,000-Dalton ν_1 polypeptide from *Torpedo marmorata* electric tissue. *Proc. Natl. Acad. Sci. USA.* 80:6403–6407.

Nickel, E., and L. T. Potter. 1973. Ultrastructure of isolated membranes of *Torpedo* electric organ. *Brain Res.* 57:508–517.

Noda, M., H. Takahashi, T. Tanabe, M. Toyosato, S. Kikiotani, Y. Furutani, T. Hirose, H. Takashima, S. Inayama, T. Miyata, and S. Numa. 1983. Structural homology of *Torpedo californica* acetyl choline receptor subunits. *Nature (Lond.).* 302:528–532.

Oberthur, W., P. Muhn, H. Baumann, F. Lottspeich, B. Wittman-Liebold, and F. Hucho. 1986. The reaction site of a non-competitive antagonist in the δ-subunit of the nicotinic actetylcholine receptor. *EMBO (Eur. Mol. Biol. Organ.) J.* 5:1815–1819.

Olek, A. J., A. Ling, and M. P. Daniels. 1986. Development of ultrastructural specializations during the formation of acetylcholine receptor aggregates on cultured myotubes. *J. Neurosci.* 6:487–497.

Peng, H. B., and S. C. Froehner. 1985. Association of the postsynaptic 43 K protein with newly formed acetylcholine receptor clusters in cultured muscle cells. *J. Cell Biol.* 100:1698–1705.

Popot, J.-L., and J.-P. Changeux. 1984. Nicotinic receptor of acetylcholine: structure of an oligomeric integral membrane protein. *Physiol. Rev.* 64: 1162–1239.

Porter, S., and S. C. Froehner. 1985. Interactions of the 43K protein with components of *Torpedo* postsynaptic membrane. *Biochemistry.* 24:425–432.

Poulter, L., J. P. Earnest, R. M. Stroud, and A. Burlingame. 1989. *Proc. Natl. Acad. Sci. USA.* In press.

Prives, J., A. B. Fulton, S. Penman, M. P. Daniels, and C. N. Christian. 1982. Interaction of the cytoskeletal framework with acetylcholine receptor on the surface of embryonic muscle cells in culture. *J. Cell Biol.* 92:231–236.

Raftery, M. A., M. W. Hunkapiller, C. D. Strader, and L. E. Hood. 1980. Acetylcholine receptor: complex of homologous subunits. *Science (Wash. DC).* 208:1454–1457.

Robinson, J. P., M. F. Schmid, D. G. Morgan, and W. Chiu. 1988. Three-dimensional structural analysis of *Tetanus* toxin by electron crystallography. *J. Mol. Biol.* 200:367–375.

Ross, M. J., M. W. Klymkowsky, D. A. Agard, and R. M. Stroud. 1977. Structural studies of a membrane-bound acetylcholine receptor from *Torpedo californica. J. Mol. Biol.* 116:635–659.

Rousselet, A., J. Cartaud, P. Devaux, and J.-P. Changeux. 1982. The rotational diffusion of the acetylcholine receptor in *Torpedo marmorata* membrane fragments studied with a spin-labelled α-toxin: importance of the 43,000 protein(s). *EMBO (Eur. Mol. Biol. Organ.) J.* 1:439–445.

Saitoh, T., L. P. Wennogle, and J.-P. Changeux. 1979. Factors regulating the susceptibility of the acetylcholine receptor protein to heat inactivation. *FEBS (Fed. Eur. Biol. Soc.) Lett.* 108:489–494.

Schofield P. R., M. G. Darlison, N. Fujita, D. R. Burt, F. A. Stephenson, H. Rodriguez, L. M. Rhee, J. Ramachandran, V. Reale, T. A. Glencorse, P. H. Seeburg, and E. A. Barnard. 1987. Sequence and functional expression of the GABAA receptor shows a ligand gated super-family. *Nature (Lond.).* 328:221–227.

Schmidt, J., and M. A. Raftery. 1973. A simple assay for the study of solubilised acetylcholine receptor. *Anal. Biochem.* 52:349–354.

Shaw, P. J., and G. J. Hills. 1981. Tilted specimen in the electron microscope: a simple specimen holder and the calculation of tilt angles for crystalline specimens. *Micron.* 12:279–282.

Stroud, R. M., and D. A. Agard. 1979. Structure determination of asymmetric membrane profiles using an iterative Fourier method. *Biophys. J.* 25:495–512.

Stroud, R. M., and J. Finer-Moore. 1985. Acetylcholine receptor structure, function and evolution. *Annu. Rev. Cell Biol.* 1:369–401.

Stya, M., and D. Axelrod. 1983. Mobility and detergent extractability of acetylcholine receptors on cultured rat myotubes: a correlation. *J. Cell Biol.* 97:48–51.

Thon, F. 1971. Phase-contrast electron microscopy. *In* Electron Microscopy in Material Science. U. Valdre, editor. Academic Press Inc., New York. 571–625.

Toyoshima, C., and N. Unwin. 1988. Ion channel of acetylcholine receptor reconstructed from images of postsynaptic membranes. *Nature (Lond.).* 336:247–250.

Unwin, P. N. T. 1975. Beef liver catalase structure: interpretation of electron micrographs. *J. Mol. Biol.* 98:235–242.

Unwin, N., C. Toyoshima, and E. Kubalek. 1988. Arrangement of the acetylcholine receptor subunits in the resting and desensitized states, determined by cryoelectron microscopy of crystallized *Torpedo* postsynaptic membranes. *J. Cell Biol.* 107:1123–1138.

Walker, J. H., C. M. Boustead, and V. Witzemann. 1984. The 43-K protein, ν_1, associated with acetylcholine receptor containing membranes is an actin-binding protein. *EMBO (Eur. Mol. Biol. Organ.) J.* 3:2287–2290.

White, B. H., and J. B. Cohen. 1988. Photolabelling of membrane-bound *Torpedo* nicotinic acetylcholine receptor with the hydrophobic probe 3-trifluoromethyl-3-(*m*-[^{125}I]iodophenyl diazirine. *Biochemistry.* 27:8741–8751.

Whiting, P., F. Esch, S. Shimasaki, and J. Lindstrom. 1987. Neuronal nicotinic acetylcholine receptor β-subunit is coded for by the cDNA clone α4. *FEBS (Fed. Eur. Biol. Soc.) Lett.* 219:459–463.

Zingsheim, H. P., F. J. Barrantes, J. Frank, W. Hanicke, and D.-Ch. Neugebauer. 1982. Direct structural localization of two-toxin recognition sites on an ACh receptor protein. *Nature (Lond.).* 299:81–84.

Ziskind-Conhaim, L., L. Geffen, and Z. Hall. 1984. Redistribution of acetylcholine receptors on developing rat myotubes. *J. Neurosci.* 4:2346–2349.